JCI insight

Detection of diabetes from whole-body MRI using deep learning

Benedikt Dietz, … , Stefan Bauer, Robert Wagner

JCI Insight. 2021;6(21):e146999. https://doi.org/10.1172/jci.insight.146999.

Research Article | Endocrinology | Metabolism

Graphical abstract

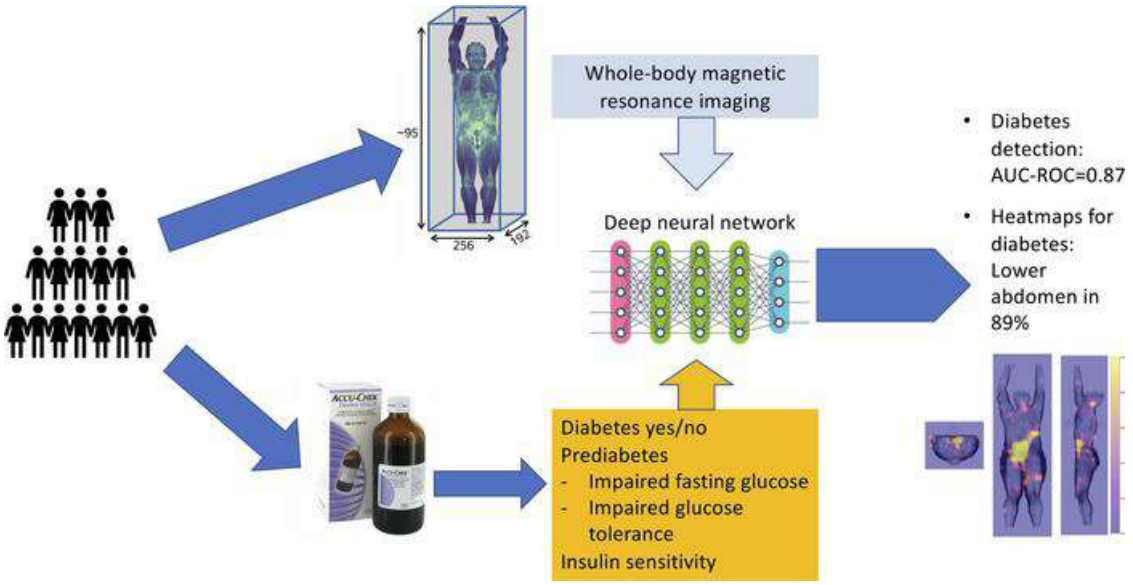

Find the latest version:

https://jci.me/146999/pdf

JCI insight

RESEARCH ARTICLE

Detection of diabetes from whole-body MRI using deep learning

Benedikt Dietz,[1] Jürgen Machann,[2,3,4] Vaibhav Agrawal,[5,6] Martin Heni,[3,4,7,8] Patrick Schwab,[9] Julia Dienes,[10] Steffen Reichert,[3,4,8] Andreas L. Birkenfeld,[3,4,8] Hans-Ulrich Häring,[3,4] Fritz Schick,[2,3,4] Norbert Stefan,[3,4,8] Andreas Fritsche,[3,4,8] Hubert Preissl,[3,4,8] Bernhard Schölkopf,[6] Stefan Bauer,[6,11] and Robert Wagner[3,4,8]

[1]Department of Computer Science, ETH Zürich, Zürich, Switzerland. [2]Department of Radiology, Section on Experimental Radiology, Eberhard-Karls University Tübingen, Tübingen, Germany. [3]Institute for Diabetes Research and Metabolic Diseases, Helmholtz Center Munich, University of Tübingen, Tübingen, Germany. [4]German Center for Diabetes Research, Neuherberg, Germany. [5]Werner Siemens Imaging Center, Tübingen, Germany. [6]Max Planck Institute for Intelligent Systems, Department of Empirical Inference, Tübingen, Germany. [7]Department for Diagnostic Laboratory Medicine, Institute for Clinical Chemistry and Pathobiochemistry, University Hospital Tübingen, Tübingen, Germany. [8]Department of Internal Medicine, Division of Diabetology, Endocrinology and Nephrology, Eberhard-Karls University Tübingen, Tübingen, Germany. [9]Institute of Robotics and Intelligent Systems, ETH Zürich, Zürich, Switzerland. [10]Department of Gynecology and Obstetrics, University Hospital Tübingen, Tübingen, Germany. [11]Department of Intelligent Systems, KTH Stockholm, Stockholm, Sweden.

Obesity is one of the main drivers of type 2 diabetes, but it is not uniformly associated with the disease. The location of fat accumulation is critical for metabolic health. Specific patterns of body fat distribution, such as visceral fat, are closely related to insulin resistance. There might be further, hitherto unknown, features of body fat distribution that could additionally contribute to the disease. We used machine learning with dense convolutional neural networks to detect diabetes-related variables from 2371 T1-weighted whole-body MRI data sets. MRI was performed in participants undergoing metabolic screening with oral glucose tolerance tests. Models were trained for sex, age, BMI, insulin sensitivity, HbA1c, and prediabetes or incident diabetes. The results were compared with those of conventional models. The area under the receiver operating characteristic curve was 87% for the type 2 diabetes discrimination and 68% for prediabetes, both superior to conventional models. Mean absolute regression errors were comparable to those of conventional models. Heatmaps showed that lower visceral abdominal regions were critical in diabetes classification. Subphenotyping revealed a group with high future diabetes and microalbuminuria risk. Our results show that diabetes is detectable from whole-body MRI without additional data. Our technique of heatmap visualization identifies plausible anatomical regions and highlights the leading role of fat accumulation in the lower abdomen in diabetes pathogenesis.

Authorship note: BD and JM contributed equally to this work and are co–first authors. SB and RW contributed equally to this work and are co–senior authors.

Conflict of interest: The authors have declared that no conflict of interest exists

Submitted: December 30, 2020
Accepted: September 29, 2021
Published: September 30, 2021

Reference information: *JCI Insight*. 2021;6(21):e146999. https://doi.org/10.1172/jci.insight.146999.

Introduction

Currently around 500 million individuals worldwide have diabetes, which has a dramatically rising prevalence (1). Most diabetes cases are type 2 diabetes, which is a condition determined by a combination of reduced insulin action in the insulin target tissues, i.e., insulin resistance, and an insufficient compensation for this insulin resistance due to an impaired insulin secretion. Epidemiologically obesity is the main driver of insulin resistance (2), but excess body fat mass is neither a prerequisite nor a guarantee for insulin resistance. There are individuals who remain metabolically healthy despite being obese (3), while others develop insulin resistance despite normal body weight (4). This is because the distribution of fat within the human body crucially determines its metabolic role. Individuals with mostly deep abdominal and visceral fat accumulation are more prone to develop insulin resistance compared with individuals with mostly subcutaneous fat deposition (5). On the other hand, subcutaneous abdominal and thigh fat seem to act as protective triglyceride dumps in the body, which preserve insulin sensitivity by confining fat to metabolically inert body regions (6, 7). Specific fat compartments, such as fat depots near arteries, seem to play distinctive roles in the pathophysiology of insulin resistance, insulin secretion, and probably also the manifestation of metabolic complications (8). Some of these perivascular fat depots, such as those near the brachial artery, have been shown to associate with insulin resistance (9). Fat tissue in the

renal sinus could contribute to nephropathy (10, 11). Furthermore, pancreatic fat deposition associates with reduced insulin secretion and may be involved in the decompensation of insulin secretion and thus in the pathogenesis of diabetes (12–14). However, it is challenging to assess the aggregate effect of fat distribution on diabetes. Simple anthropometric variables of fat distribution, such as waist and hip circumference, are not very accurate and provide only limited information on the distribution of fat over the body. A more accurate measurement of fat distribution can be achieved by whole-body T1-weighted MRI (15), which by design contrasts fat and water signals as a distribution of gray scale voxels over the body. It is possible to perform a segmentation of MR images to quantify specific predetermined regions, but this approach is laborious and could be biased by predefined areas of interest. We therefore investigated if 3-dimensional whole-body MR tomograms could be applied in an unbiased way to determine if the represented individual had diabetes at the time of the scan. Adequately trained machine-learning models have recently been very successful in associating high-dimensional data with medical labels (16). Although it is notoriously challenging to derive human-readable information on key patterns of machine-learning classifiers (17), we also aimed to extract information on the anatomical regions decisive in establishing these associations.

Results

Model training for diabetes and related labels. Sex classification converged to approximately 99% area under the receiver operating characteristic curve (AUROC) within the first approximately 25 epochs on the training set. All other labels tended to take considerably longer to converge, and individual performances varied with different network parameters. While sex classification seemed to be easily feasible for the network, the smoothed AUROC scores for the diabetes labels mostly peaked at approximately 85% for diabetes and approximately 70% for prediabetes and the extended diabetes label. As for the regression tasks, all of the predictive performances slightly varied. However, with different network parameters they generally converged to approximately 5%–15% mean absolute error (MAE) on the normalized training labels before starting to overfit. In all models, the lowest MAE has been reached for the estimation of BMI. The results of classifications and regressions achieved by the potentially novel dense convolutional neural networks in the optimal model are shown in Table 1.

The AUROC for classification of diabetes was 0.87. Receiver operator characteristics curves with and without stratification for sex are shown in Figure 1. As a comparison for the dense convolutional neural networks, conventional models were trained using body fat volumes determined by fat compartment segmentation.

A normalized MAE of 0.17 for age is equivalent to ±10 years average error. Similarly, a normalized BMI MAE of 0.07 represents an average error of ± 2kg/m^2, and 0.13 normalized HbA1c MAE equals ±0.4%. Finally, the insulin sensitivity error of 0.26 corresponds to an average error of ±10.2 AU, which represents the weakest regression performance among the continuous outcome variables.

Sensitivity analyses with different model setups. We also tested the diagnostic precision of different model setups for the labels sex, prediabetes, and diabetes and the diabetes label extended by impaired fasting glucose and impaired glucose tolerance (IFG+IGT) (Supplemental Table 2; supplemental material available online with this article; https://doi.org/10.1172/jci.insight.146999DS1). Part of these alternative models used images cropped to torso only or abdomen only (Supplemental Figure 3). As additional augmentation technique, we tested random zooming on the images. Detection of sex was not affected by the restricted images, but the diabetes and prediabetes labels reached lower AUROC values. Interestingly, diabetes detection was only slightly affected when using abdominal images, and these techniques had no relevant effect on the detection of diabetes with IFG+IGT. With model training rerun using only the first scan from each participant, we yielded lower AUROC for diabetes, but the prediabetes and the extended diabetes labels showed comparable diagnostic precision to the original data set.

Target-specific gradient maps. We computed attention heatmaps to acquire information about the reasoning behind predictions and to provide visualizations for further analyses. Comparison plots of heatmaps for 50 randomly selected samples for the detection of diabetes and insulin sensitivity are shown in Figure 2A The highlighted areas were assigned to prespecified anatomic regions by 3 clinicians who had expertise in the interpretation of medical imaging. For each of the 8 traits, the human experts rated 100 images presented in 3 dimensions (see example in Figure 2B). Interrater agreement was 76%.

Mean percentages for the predefined anatomical regions appearing in the heatmaps are shown in Table 2. The deep lower abdominal (visceral) region was associated with most cases of diabetes classification

Table 1. Model performance metrics

Model	Classification (AUROC)				Regression (MAE)			
	Sex	Diabetes	Prediabetes	Diabetes with IFG+IGT	Age	BMI	Matsuda-index	HbA1c
DCN	0.99	0.87	0.68	0.72	0.17	0.07	0.26	0.13
LR/KN		0.54	0.51	0.63	0.193	0.075	0.143	0.135
RF		0.51	0.59	0.56	0.19	0.07	0.142	0.14
SVM		0.60	0.51	0.42	0.192	0.07	0.141	0.134

Summary of model performance metrics for the final dense convolutional network (DCN) compared, with conventional classifiers (LR, linear regression; KN, K-neighbors classifier; RF, random forest; SVM, support vector machine) used as benchmarks. Model performance is shown as area under the receiver operator characteristics curve (AUROC) for classification and mean absolute error (MAE) for regression.

(89%). This region also seemed to be important, however, less prominent, for classifying diabetes with IFG+IGT cases (84%) and prediabetes cases (69%). For the classification of sex, the upper thorax region, including the breasts, played the major role (73% highlighted). Arms and upper legs were also important (67 and 61%, respectively). The upper leg region was also often highlighted in the heatmaps of the regression on BMI (64%) and insulin sensitivity (70%).

Clusters based on the embedding layer of MRI scans. Of the highly complex MRI scans, the training process generated vectors with 128 values per image. These are called embeddings and contain all relevant information from the scans. To investigate whether this information contained in whole-body MRI scans can be used for the prediction of metabolic features, we performed sex-stratified data-driven clustering on the embeddings. The clusters solely based on data from the embeddings delineated groups with different anthropometric and glycemic features (Figure 3, A and B, and Table 3). Furthermore, they also predicted future diabetes (Figure 3C, $n = 586$ with follow-up data, mean follow-up 4 ± 3.7 years, number of events = 48, $P < 0.0001$) and the development of microalbuminuria (Figure 3D, $n = 550$ with follow-up data, mean follow-up 4.3 ± 3.6 years, number of events = 95, $P = 0.004$). Anthropometric variables were different across clusters, but the association of cluster 4 with increased risk of diabetes and microalbuminuria was still significant after adjustment for sex, age and BMI ($P = 0.01$ and $P = 0.03$, respectively). In addition, the association of cluster 4 with these outcomes was not explained by differences in baseline glycemia ($P = 0.02$ for future diabetes after adjusting for baseline glycated hemoglobin) or baseline urinary albumin-to-creatinine ratio (uACR) ($P = 0.04$ for future microalbuminuria after adjusting for baseline uACR, $n = 441$, events = 76).

Discussion

Here, we tested if presence of diabetes can be identified from specific patterns of body fat distribution assessed by MRI. With a machine-learning approach on more than 2000 whole-body MRI data sets, we produced excellent classification results that were superior to those from state-of-the-art statistical modeling of body fat compartment volumes. These results prove that diabetes is detectable with deep learning from imaging data. Accordingly, 3-dimensional MRI images harbor patterns for a sufficiently good discrimination of patients with and without diabetes. Of note, the images were normalized for body length to target a classification based on fat distribution rather than body height.

In an empirical approach to look into the black box of machine learning, we applied human expert rating of heatmaps representing regions important for classification and regression. The interpretation of these heatmaps suggests that deep lower abdominal fat was most critical for the detection of diabetes by the machine (89% of diabetes heatmaps contained these areas). Furthermore, we also detected diabetes-related signals in the upper legs (66%), the arms (51%), and the neck region (51%).

Visceral fat, in contrast to subcutaneous fat, has been previously identified as an important predictor of insulin resistance, the failure to respond to lifestyle intervention and the future manifestation of diabetes (18, 19). Interestingly and somewhat unexpectedly, structures in the lower rather than upper abdomen turned out to be the most important topographic areas in our analyses. These results suggest that not all visceral adipocytes have the same impact on metabolism and point toward a heterogeneity with metabolically unfavorable fat enriched in the lower part. Highlights in the neck region could be linked to insulin resistance.

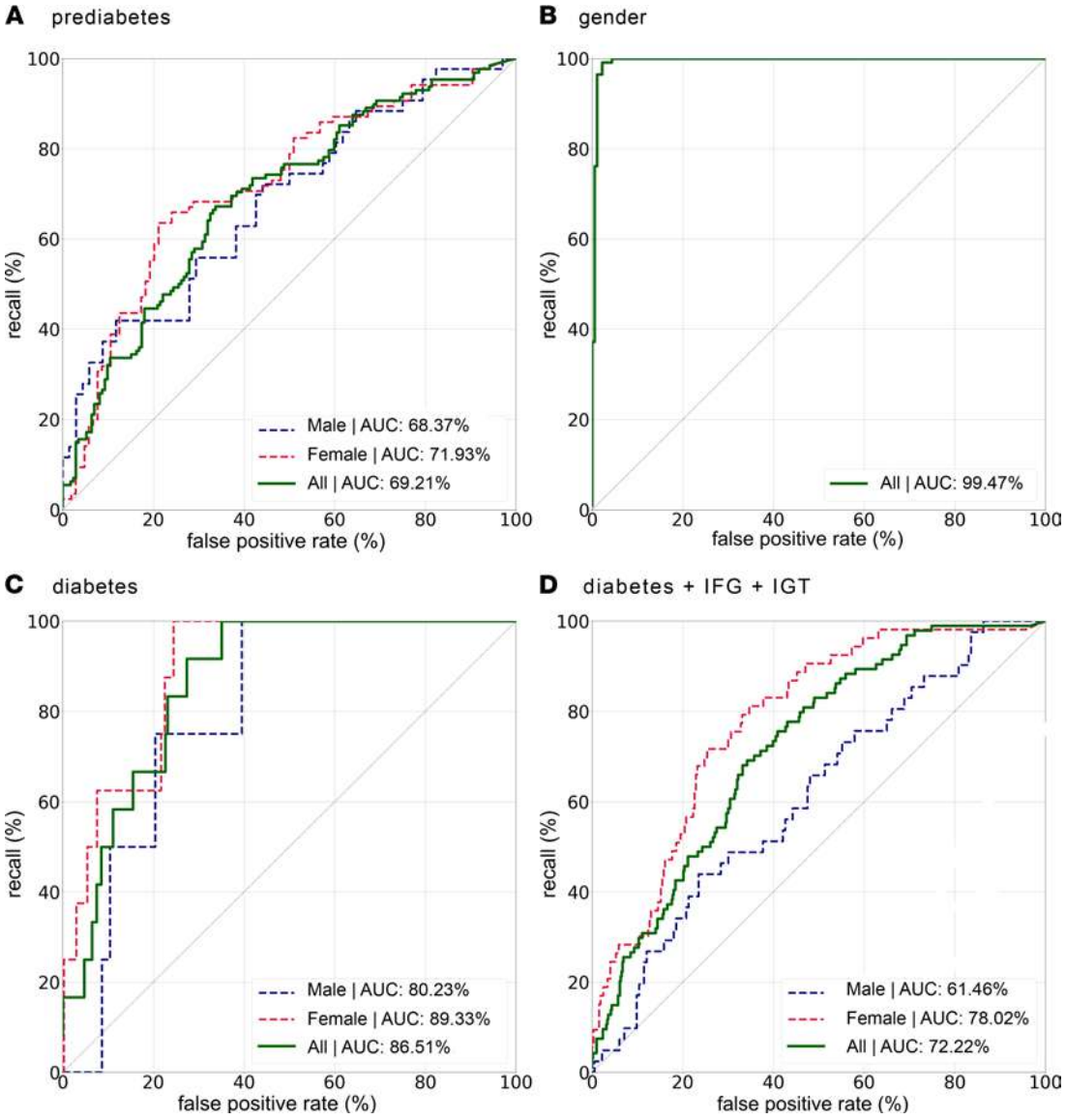

Figure 1. Diagnostic accuracy of the machine-learning classifiers. Receiver operating characteristic curves for the detection of prediabetes (**A**), sex (**B**), diabetes (**C**), and diabetes with impaired fasting glucose and impaired glucose tolerance (diabetes+ IFG + IGT, **D**) by the dense convolutional neural network.

Indeed, interscapular fat had been shown as an important independent marker of insulin resistance (20). Its importance in diabetes pathology is corroborated by our current hypothesis-free approach. The arms and upper leg regions are unforeseen hot spots, because they mostly comprise subcutaneous, metabolically inert fat depots. For estimation of BMI, arms and upper legs were the leading anatomic regions and might therefore predominantly represent general obesity. Of note, the upper leg region was also leading in the regression for insulin sensitivity (featured in 70% of heatmaps). Insulin resistance is the major body fat–derived metabolic factor in the pathogenesis of diabetes. However, insulin resistance is by itself not sufficient to cause diabetes (21). Diabetes only manifests if there is an additional disruption of pancreatic insulin secretion. Accordingly, we see a clear dissociation of the diabetes- and insulin resistance–related regions in our heatmaps. Unexpectedly, the deep lower abdomen differentiated diabetes from solitary insulin resistance. As the pancreas is not located in this area, our results suggest that additional biological signals that originate from the lower abdomen and target pancreatic islets could impair insulin release. The pancreas probably did not emerge directly in our machine-learning approach, as diabetes-related changes only occur in the islets that represent a minute proportion of the entire organ and can therefore hardly be detected by imaging. Another organ with known important contribution to diabetes, the liver, could correspond

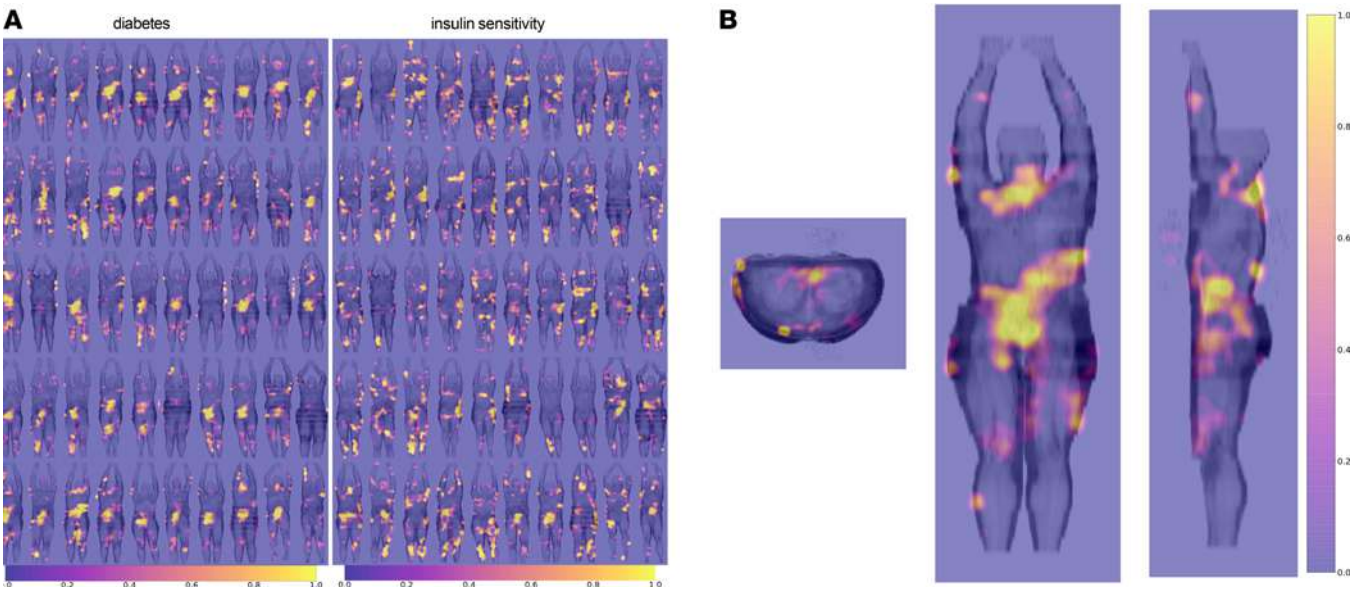

Figure 2. Gradient maps visualizing voxels with large influence on the classification/regression outcome. (**A**) Gradient maps for diabetes and insulin sensitivity, computed for 50, randomly selected, persons with prediabetes. The body scans, as well as the gradient maps, were averaged along the coronal projection to generate 2-dimensional representations. (**B**) An example gradient heatmap for the diabetes label in 3 projections. For assignment of gradient maps to body regions by raters, similar 3-dimensional gradient map representations, were used.

to highlighted areas in the deep right upper abdomen, appearing in 64% of diabetes with IFG+IGT classifiers. Accordingly, there was considerably less highlighting in the left upper abdomen, i.e., outside of the liver (13%). We have previously shown that a disruptive organ crosstalk among fat, liver, and pancreatic β cells could contribute to a deterioration of insulin secretion (13). Our findings about diabetes-related features of whole-body MRI stress the multiorgan nature of diabetes pathology.

The cluster analysis of the embeddings generated by machine learning from MRI scans shows a clear discrimination of 4 groups. This is not just a sole clustering of random image information but has biological meaning, as the clusters delineate different demographic and metabolic entities. As one of the identified subphenotypes was also associated with future diabetes and microalbuminuria, the most important early marker of diabetic kidney disease, the information content of the MRI images is also highly relevant for prediction of glycemic deterioration and a diabetes complication.

The results of sensitivity analyses using images restricted to the abdominal region suggest that future investigations could mainly focus on abdominal MR imaging. Using state-of-the art MR imaging techniques, higher resolution and faster acquisition times could be yielded, which might contribute to a better understanding of abdominal anatomy to diabetes pathology.

Our work has some limitations. Although different scanners were used to produce our data, this was a single-center study without external replication. Despite splitting our data into training, test, and replication sets, how our classifier will perform on data from different centers still needs to be tested. Furthermore, some of the data were repeated measurements in the same person, which we were unable to explicitly address in the machine-learning procedure. However, labels were updated concurrently (from oral glucose tolerance tests [OGTTs] performed at the time of each MRI scan), linking the respective metabolic status to anatomic patterns, and sensitivity analyses using a subset of the data without repeated measurements show comparable results for some labels. Capturing the intuition behind machine learning is still challenging, and there is no generally accepted method for this. To our knowledge, this is the first work to utilize 3-dimensional MRI whole-body scans for the analysis of diabetes and related features as well as to investigate a combination of heatmaps and their assignment to anatomic hot spots by human experts.

In summary, our work provides evidence that machine learning can classify diabetes from whole-body MRI. Diabetes, but not insulin sensitivity, was particularly associated with the features of the deep lower abdomen. This points toward considerable heterogeneity in the metabolic role of fat located in different parts of the visceral adipose tissue that has not been described so far. Further research is warranted on underlying molecular pathways that could represent important novel pathomechanisms in diabetes development.

Table 2. Human expert classification of gradient heatmaps generated from the output nodes of the machine-learning classifier network

		Arms	Head	Lower legs	Upper legs	Lower abdominal visceral region	Mediastinum	Neck	Thighs, lower abdominal s.c. regions	Abdomen, upper left visceral region	Abdomen, upper right visceral region	Breasts, upper thorax
1	Sex	67%	28%	51%	61%	42%	10%	12%	45%	5%	17%	73%
2	Age	46%	5%	34%	63%	62%	1%	46%	50%	11%	31%	13%
3	BMI	62%	2%	22%	64%	19%	9%	29%	60%	44%	36%	39%
4	Diabetes	51%	14%	28%	66%	89%	4%	50%	27%	14%	42%	12%
5	Diabetes and IFG+IGT	44%	8%	16%	49%	84%	2%	51%	22%	13%	64%	7%
6	Prediabetes	49%	4%	31%	53%	69%	1%	50%	20%	12%	59%	12%
7	HbA1c	64%	24%	36%	40%	62%	4%	42%	30%	5%	38%	23%
8	Insulin sensitivity	45%	38%	61%	70%	22%	9%	6%	51%	4%	14%	51%

The values show the mean percentage of an anatomical region appearing in the heatmaps of a given trait.

Methods

Study population and MRI

MRI was performed on individuals who participated in metabolic screenings within the framework of multiple studies performed at the Department of Medicine IV, University Hospital Tübingen. In most of these studies, participants were generally healthy, without known type 2 diabetes but with an increased risk for the disease. This was defined as either family history of type 2 diabetes, BMI of greater than 27 kg/m^2, or known prediabetes. The participants came fasted to the study facility and underwent whole-body MRI in the early morning, which was followed by a health examination, assessment of medical history, and an OGTT. OGTT does not only allow assessment of insulin sensitivity and glucose tolerance, but it is also the gold-standard detection of diabetes. Follow-up data for diabetes incidence and assessment of complications such as microalbuminuria was available for a subset of the subjects.

During the MRI, subjects were lying in a prone position with extended arms, and images were recorded from fingers to toes. A T1-weighted fast spin–echo technique with a slice thickness and an interslice gap of 10 mm was applied, allowing discrimination of adipose and lean tissue due to inherent different longitudinal relaxation times T1. The patient table was shifted by 10 cm after each measurement (12 seconds each). Total acquisition time, including 1 rearrangement, was 20–25 minutes (15).

Data acquisition

Within the whole-body MRI scanning procedure, 90–120 parallel transverse slices were generated per participant, depending on body height. We quantified total adipose tissue volume, visceral adipose tissue volume, and upper extremities adipose tissue volume from these images for the benchmark models, using methods described previously (22). MR voxel arrays were provided in the Digital Imaging and Communications in Medicine file format. The original data set consisted of 2555 whole-body scans of 1080 participants, as some had been scanned multiple times. The number of MRI scans involved at different steps of the analysis is shown in Supplemental Figure 1. We used 8 ground truth labels. Four of these were binary labels; 1 was for sex, and the remaining 3 were for different diabetes definitions, including diabetes (Dα), prediabetes (Dβ), and a third definition, Dγ, that denoted diabetes cases extended with participants having concomitant IFG and IGT. In addition to the 4 binary labels, we used age (years), BMI (kg/m^2), insulin sensitivity (determined with the Matsuda index; ref. 23), and glycated hemoglobin (HbA1c) (%) as target labels for the network. An overview of the characteristics of participants and the labels is provided in Supplemental Table 1. Laboratory measurements were performed as previously described (24). The diagnosis of diabetes was established by one of the following: fasting glucose >7.0 mmol/l, postchallenge glucose ≥11.1 mmol/l or a glycated hemoglobin ≥48 mmol/mol. Microalbuminuria was established by a uACR ≥30 mg/g creatinine.

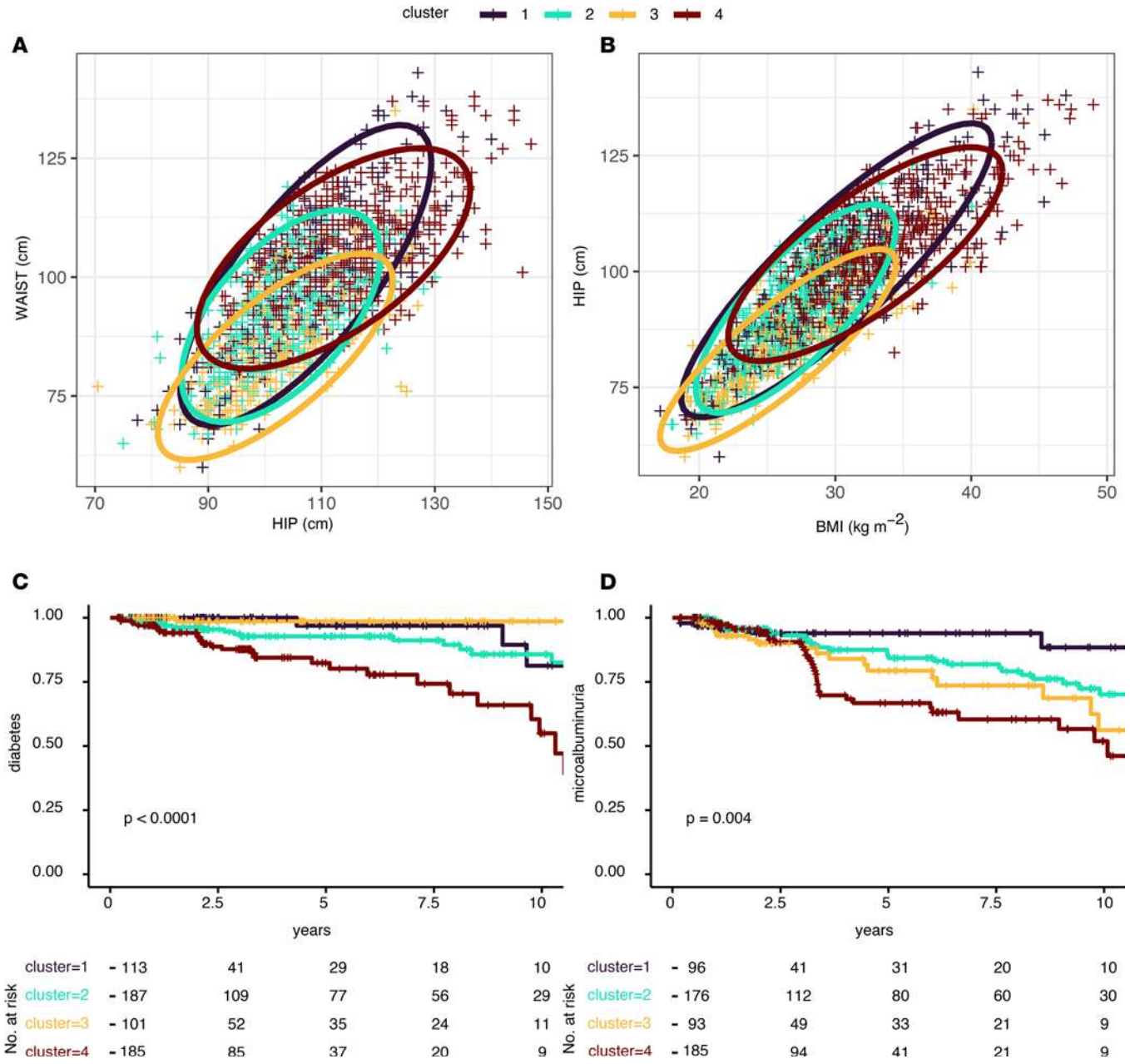

Figure 3. Partitioning of MRI images. Data-driven clustering was performed from embedding layers, which are numeric representations of MRI scans generated during inference (n = 2048). The MRI-based clusters have different distributions of waist and hip circumference (**A**) and BMI (**B**). For the participants with follow-up data, these MRI-data based clusters also define different risk profiles not only for new-onset diabetes (n = 586) (**C**), but also for the diabetes complication microalbuminuria (n = 550) (**D**). Diagrams showing incidence-free survival were compared with log-rank tests.

Data preprocessing

Shape normalization. As mentioned, MRI scans were acquired by generating image slices along the body's horizontal plane. Unlike the slice dimension, the number of slices varied according to body height. The most frequent number of slices was 95. All scans with different heights were linearly interpolated along the vertical body axis to produce volumes with normalized dimensions of 95 × 150 × 250 voxels. The voxel grid resolution of the 2 horizontal axes (considering a standing person) was considerably higher than the resolution along the body height axis, with negligible differences in coronal (z axis) scaling due to the aforementioned interpolation. We did not correct the lower resolution on the axis corresponding to the body height with further interpolations. However, we downsampled the standardized voxel grids for computational efficiency to their final dimension of 85 × 110 × 135 voxels.

Table 3. Characteristics of clusters generated from embedding layer representation of the MRI scans

	Clusters				
	1	2	3	4	*P* value
n	366	663	341	678	
Male sex (%)	251 (68.6)	280 (42.2)	40 (11.7)	217 (32.0)	<0.001
Female sex (%)	115 (31.4)	383 (57.8)	301 (88.3)	461 (68.0)	
Age in yrs (mean [SD])	42.94 (11.90)	55.14 (10.62)	37.72 (10.86)	55.66 (9.95)	<0.001
BMI (kg/m^2) (mean [SD])	30.44 (5.56)	27.13 (3.43)	26.23 (4.18)	32.47 (4.82)	<0.001
Waist circumference (cm) (mean [SD])	100.33 (14.79)	91.83 (10.14)	84.36 (10.63)	104.23 (11.08)	<0.001
Hip circumference (cm) (mean [SD])	107.73 (10.98)	103.11 (8.28)	102.33 (10.01)	112.51 (11.13)	<0.001
Total adipose tissue MRI (L) (mean [SD])	35.61 (14.44)	28.62 (8.71)	28.57 (9.50)	41.35 (12.57)	<0.001
s.c. adipose tissue MRI (L) (mean [SD])	11.91 (6.69)	8.96 (3.98)	8.56 (3.93)	14.96 (6.36)	<0.001
Visceral adipose tissue MRI (L) (mean [SD])	4.34 (2.57)	3.43 (1.84)	1.53 (1.25)	5.01 (2.03)	<0.001
s.c.-to-visceral adipose ratio (mean [SD])	3.44 (2.25)	3.25 (1.94)	7.23 (3.62)	3.45 (1.96)	<0.001
Visceral adipose % of total (mean [SD])	0.12 (0.06)	0.12 (0.06)	0.05 (0.04)	0.13 (0.06)	<0.001
% Liver fat content (mean [SD])	6.02 (5.68)	4.40 (4.32)	2.25 (2.80)	9.55 (7.67)	<0.001
% Fatty liver disease (mean [SD])	138 (37.9)	165 (25.4)	26 (7.8)	381 (57.0)	<0.001
Systolic blood pressure (mmHg) (mean [SD])	131.19 (16.20)	129.95 (16.32)	120.52 (13.73)	137.71 (16.60)	<0.001
Diastolic blood pressure (mmHg) (mean [SD])	83.25 (11.87)	81.38 (10.95)	76.73 (10.09)	87.62 (11.28)	<0.001
Heart rate (bpm) (mean [SD])	68.57 (12.57)	67.98 (10.49)	69.80 (10.61)	71.64 (10.24)	<0.001
Fasting glucose (mmol/l) (mean [SD])	5.30 (0.51)	5.43 (0.52)	5.02 (0.40)	5.65 (0.61)	<0.001
Postchallenge glucose (mmol/l) (mean [SD])	6.47 (1.53)	6.95 (1.77)	6.13 (1.46)	7.61 (2.10)	<0.001
Glycemic category					<0.001
NGT (%)	237 (64.8)	348 (52.5)	272 (79.8)	246 (36.3)	
IFG (%)	63 (17.2)	136 (20.5)	29 (8.5)	147 (21.7)	
IGT (%)	38 (10.4)	90 (13.6)	37 (10.9)	98 (14.5)	
IFG+IGT (%)	25 (6.8)	57 (8.6)	2 (0.6)	108 (15.9)	
DIA (%)	3 (0.8)	32 (4.8)	1 (0.3)	79 (11.7)	
Glycated hemoglobin (mmol/mol) (mean [SD])	36.36 (3.59)	38.52 (4.00)	35.29 (3.49)	39.86 (4.27)	<0.001
Triglycerides (mmol/l) (mean [SD])	1.36 (0.80)	1.30 (0.73)	1.03 (0.56)	1.70 (1.51)	<0.001
Insulin sensitivity (Matsuda, arbitrary units) (mean [SD])	14.80 (10.17)	15.63 (8.75)	19.50 (9.29)	8.91 (5.07)	<0.001
Fasting insulin (pmol/l) (mean [SD])	64.55 (41.69)	51.20 (32.15)	46.90 (26.86)	86.24 (47.78)	<0.001
Insulinogenic index (arbitrary units) (mean [SD])	145.93 (137.84)	96.31 (83.69)	139.64 (184.45)	130.14 (99.14)	<0.001
Disposition index (arbitrary units) (mean [SD])	1781.41 (3409.53)	1287.56 (1252.09)	2834.08 (6596.89)	990.99 (852.42)	<0.001
C-reactive protein (mg/dl) (mean [SD])	0.20 (0.30)	0.18 (0.27)	0.23 (0.35)	0.41 (0.50)	<0.001
Cholesterol (mmol/l) (mean [SD])	4.96 (0.94)	5.22 (0.93)	4.58 (0.86)	5.28 (1.01)	<0.001
LDL (mmol/l) (mean [SD])	3.07 (0.85)	3.18 (0.78)	2.66 (0.79)	3.21 (0.85)	<0.001
HDL (mmol/l) (mean [SD])	1.27 (0.33)	1.43 (0.34)	1.48 (0.32)	1.34 (0.32)	<0.001
Aspartate aminotransferase (U/l) (mean [SD])	26.85 (20.34)	23.68 (8.16)	20.76 (8.40)	25.17 (9.88)	<0.001
Alanine aminotransferase (U/l) (mean [SD])	32.69 (18.81)	24.31 (11.90)	19.91 (12.18)	30.38 (17.05)	<0.001
γ-Glutamyl transferase (U/l) (mean [SD])	30.63 (21.11)	25.55 (24.48)	15.94 (15.55)	34.30 (29.85)	<0.001
Serum creatinine (mg/dl) (mean [SD])	0.85 (0.16)	0.83 (0.16)	0.78 (0.15)	0.78 (0.16)	<0.001
Urine albumin-creatinine ratio (mean [SD])	24.48 (107.36)	18.50 (46.32)	21.20 (37.48)	20.69 (37.70)	0.558

Anthropometric, clinical, and laboratory characteristics of clusters generated from embedding layer representation of the MRI scans. DIA, diabetes; NGT, normal glucose tolerance; IFG, impaired fasting glucose; IGT, impaired glucose tolerance.

Voxel value normalization. Voxels that did not belong to the body (e.g., caused by motion artifacts inherent to MRI) were identified using value distributions and set to 0. We standardized body voxel values to have a mean of 0 and a SD of 1 and truncated and subsequently shifted the distribution to strictly positive values to keep the distinction from the surrounding air. We transformed all scan samples equally.

Labels

A total of 8 outcome label variables were used as described. Samples with missing labels were excluded, continuous variables were normalized to a range between 0 and 1. Outliers were removed using the isolation

forest algorithm and fitted on a subset of the medical features, namely insulin sensitivity, BMI, HbA1c, as well as total adipose tissue estimate (25).

Data partitioning

In order to assess the generalization capabilities of our models, we applied a stratified random split to separate the entire data set into training (70%), validation (15%), and test (15% of all data) folds. The folds were stratified by BMI, insulin sensitivity, and diabetes. Our stratification algorithm required that each multivariate stratum contains more than 1 sample (Supplemental Figure 1).

Augmentation

To increase model robustness, the input volumes were augmented in several ways. Additional 0 padding was added to each dimension, increasing the size of the 3-dimensional image array. To augment the training samples, the degree of padding was dynamically adjusted at random during training. Furthermore, a series of rotations were randomly performed on each input array as well as addition of Gaussian noise to all body voxels (Supplemental Figure 2). For testing and validation, the body volumes were centered, and no rotation or noise was applied. We also performed sensitivity analyses using additional random zooming of the images during the training. Furthermore, we tested the training on restricted images cropped to the torso and abdominal area (Supplemental Figure 3, A and B).

Model architecture

Densely connected convolutional layers. We built the network in accordance to the DenseNet architecture (26). The 3-dimensional input volumes were fed to the input layer in batches consisting of 8 samples each. The initial layer consisted of a fully connected convolutional layer with a kernel size of 5 and 8 convolutional filters. The initial convolutional layer was followed by a batch normalization layer (27, 28). The dimensions of the intermediary feature maps were subsequently downsampled using a pooling layer to improve computation efficiency. The output was fed to the first dense block. Alternating dense blocks and transition layers were sequentially added to process the input.

Following the final transition layer, the activation maps were flattened to a 1-dimensional array and passed to 3 sequential densely connected layers with dropout. The output of the dense layers had the dimension 1 × 128 units and was referred to as the embedding layer, embodying low-dimensional representations of MRI voxels as "learned" by the neural network. The embedding layer was used for the prediction of the desired target labels and for unsupervised clustering analysis. For the prediction of the output nodes, subsequent dense layers were added to the embedding layer. A schematic of the entire model is provided in Supplemental Figure 2.

Gradient heatmaps. Predictions for the various target variables were directly represented by the output nodes. Differentiating these with respect to previous convolutional layers yields pixel-wise gradients. The chosen approach for heatmap generation was gradients × input (27); hence, we computed the gradients of the individual outputs with respect to the image input. Differentiating resulted in target-specific gradients of the same dimension as the input scans. Gradient heat maps were assigned to anatomical regions by 3 human medical experts (experienced physicians working in hospitals) who had experience in the evaluation and interpretation of medical imaging. All expert raters were blinded to the subject characteristics as well as to the trait they rated. Results were averaged for the 3 raters.

Hyperparameters. We used a growth factor kGrowth = 18. The initial convolution layer, prior to the first dense block had a kernel size of 5 × 5 × 5 voxels, and it generated 4 activation maps. We chose to evaluate the model with 3 dense blocks and 3 subsequent fully connected layers, downsampling the flattened representation to 512, 256, and 128, respectively. With the sole exception of the final regression output layers, all activation functions throughout the network were exponential linear units (28). We chose the initialization proposed by He et al. (29) for all kernel weights. Adam (30) was used as optimizer with an initial learning rate of 10-4. All other hyperparameters of the optimizer were kept at their Tensorflow (31) implementation defaults. The learning rate is adapted during training through a Tensorflow variable and has a cyclic, exponentially decay.

Training. Network training was performed on a Nvidia Tesla V100-PCIE 32GB GPU, using the CUDA framework (32). The network was trained for a maximum of 250 epochs with a batch size of 8, due to the considerable memory requirements of our 3-dimensional voxel grids. The network converged after approximately 2–3 days, depending on network depth, i.e., number of trainable parameters as well as batch size and other hyperparameters.

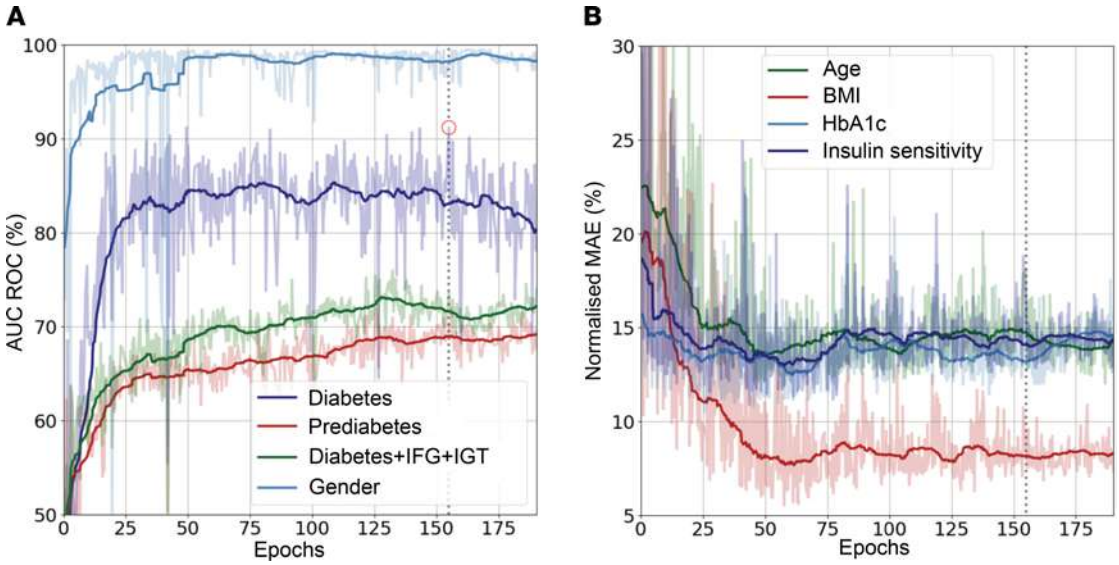

Figure 4. Training metrics and model selection. Performance of models in subsequent computation runs for classifications (area under the receiver operating characteristic (ROC) curves (**A**) and regressions (normalized mean absolute error) (**B**). The circled point in **A** indicates the highest achieved ROC for diabetes in the validation set.

Model selection. We frequently evaluated the network's performance and selected the model according to the highest diabetes (Dα) AUROC score on the validation set.

We first summarized the training progress, using the AUROC and MAE metric on the validation set over all trained epochs (Figure 4). Metrics were generally computed on the test set with the exception of diabetes (Dα) and prediabetes (Dβ). Due to the critically low number of positives for these labels, we chose to concatenate the data sets for testing and validation to compute the classification performance metrics. To assess the performance of our approach, benchmark models were computed using linear regression and k-nearest neighbor classifier, random forest models, and support vector machines for comparison. Body fat compartment volumes that have been segmented from MR images (total, visceral, and upper limb adipose tissue) were used as model inputs.

Postprocessing. The output of the model consisted of a set of predictions for each sample in addition to the respective gradient maps as well as its embedding space representation.

We used gradient maps to compute target specific heat maps, using the gradients×input method, proposed by Shrikumar et al. (27). The individual output nodes were differentiated with respect to the input to produce 3-dimensional feature-specific gradient maps. For visualization, the gradient maps were postprocessed using Gaussian filters in addition to contrast enhancements and averaging to 2 dimensions. Furthermore, for the classification nodes, only the output node corresponding to the correct label was considered. In other words, for a patient with label female, only the gradient that increased the female probability prediction was used for visualization. All positive gradients were considered for the regression tasks.

Data availability

All requests for data and materials are promptly reviewed by the Data Access Steering Committee of the Institute of Diabetes and Metabolic Research, Tübingen, Germany, to verify if the request is subject to any intellectual property or confidentiality obligations. Individual level data may be subject to confidentiality. Any data and materials that can be shared will be released via a material transfer agreement.

Statistics

Cluster analysis was performed on the embeddings using partitioning around medoids with Gower's distances. The optimal number of clusters was selected using average Silhouette widths. To investigate the robustness of the clusters, we performed a bootstrap validation showing a Jaccard similarity index of 0.73 over all clusters. A subset of the participants was tested during follow-up visits for incident diabetes (n = 586) and microalbuminuria (n = 550). Comparison of risks was performed using Kaplan-Meier diagrams and log-rank tests. Further analyses with adjustments for potential confounders were performed with proportional hazards models. Proportional hazards assumptions were tested by visualizing Schoenfeld residuals.

Study approval

The studies were carried out with written informed consent from all subjects in accordance with the Declaration of Helsinki. All protocols were approved by the ethics committee of the University of Tübingen.

Author contributions

JM and RW contributed to data acquisition, analyzed the data, and wrote the manuscript. BD, VA, and SB analyzed the data and wrote the manuscript. JD and SR contributed to data acquisition and the interpretation of data and edited the manuscript. MH, HUH, and AF contributed to the concept of the work and edited the manuscript. PS, ALB, FS, NS, HP, and BS contributed to the interpretation of data and edited the manuscript. All authors have reviewed the manuscript. BD constructed the first machine-learning models and is therefore listed first among the co–first authors.

Acknowledgments

This study was supported in parts by a grant (01GI0925) from the Federal Ministry of Education and Research to the German Center for Diabetes Research and from the state of Baden-Württemberg (32-5400/58/2, Forum Gesundheitsstandort Baden-Württemberg). We thank all the research volunteers for their participation. We gratefully acknowledge the excellent technical assistance of the Diabetes Research Unit Diabetes Research and Metabolic Diseases of the Helmholtz Center Munich at the University of Tübingen. We thank Benjamin A. Jaghutriz, University Hospital Tübingen, for his help in heatmap assignment.

Address correspondence to: Robert Wagner, Otfried-Müller-Str 10, 72076 Tübingen, Germany. Phone: 49.7071.2968967; Email: robert.wagner@med.uni-tuebingen.de.

1. Chatterjee S, et al. Type 2 diabetes. *Lancet*. 2017;389(10085):2239–2251.
2. Kahn BB, Flier JS. Obesity and insulin resistance. *J Clin Invest*. 2000;106(4):473–481.
3. Stefan N, et al. Identification and characterization of metabolically benign obesity in humans. *Arch Intern Med*. 2008;168(15):1609–1616.
4. Stefan N, et al. Causes, characteristics, and consequences of metabolically unhealthy normal weight in humans. *Cell Metab*. 2017;26(2):292–300.
5. Goodpaster BH, et al. Subcutaneous abdominal fat and thigh muscle composition predict insulin sensitivity independently of visceral fat. *Diabetes*. 1997;46(10):1579–1585.
6. Stefan N, et al. Metabolically healthy obesity: the low-hanging fruit in obesity treatment? *Lancet Diabetes Endocrinol*. 2018;6(3):249–258.
7. McLaughlin T, et al. Preferential fat deposition in subcutaneous versus visceral depots is associated with insulin sensitivity. *J Clin Endocrinol Metab*. 2011;96(11):E1756–E1760.
8. Siegel-Axel DI, Häring H-U. Perivascular adipose tissue: an unique fat compartment relevant for the cardiometabolic syndrome. *Rev Endocr Metab Disord*. 2016;17(1):51–60.
9. Rittig K, et al. Perivascular fatty tissue at the brachial artery is linked to insulin resistance but not to local endothelial dysfunction. *Diabetologia*. 2008;51(11):2093–2099.
10. Wagner R, et al. Exercise-induced albuminuria is associated with perivascular renal sinus fat in individuals at increased risk of type 2 diabetes. *Diabetologia*. 2012;55(7):2054–2058.
11. Wagner R, et al. The protective effect of human renal sinus fat on glomerular cells is reversed by the hepatokine fetuin-A. *Sci Rep*. 2017;7(1):2261.
12. Heni M, et al. Pancreatic fat is negatively associated with insulin secretion in individuals with impaired fasting glucose and/or impaired glucose tolerance: a nuclear magnetic resonance study. *Diabetes Metab Res Rev*. 2010;26(3):200–205.
13. Gerst F, et al. Metabolic crosstalk between fatty pancreas and fatty liver: effects on local inflammation and insulin secretion. *Diabetologia*. 2017;60(11):2240–2251.
14. Gerst F, et al. What role do fat cells play in pancreatic tissue? *Mol Metab*. 2019;25:1–10.
15. Machann J, et al. Follow-up whole-body assessment of adipose tissue compartments during a lifestyle intervention in a large cohort at increased risk for type 2 diabetes. *Radiology*. 2010;257(2):353–363.
16. Rajkomar A, et al. Machine learning in medicine. *N Engl J Med*. 2019;380(14):1347–1358.
17. Holm EA. In defense of the black box. *Science*. 2019;364(6435):26–27.
18. Hayashi T, et al. Visceral adiposity, not abdominal subcutaneous fat area, is associated with an increase in future insulin resistance in Japanese Americans. *Diabetes*. 2008;57(5):1269–1275.
19. Thamer C, et al. High visceral fat mass and high liver fat are associated with resistance to lifestyle intervention. *Obesity (Silver Spring)*. 2007;15(2):531–538.
20. Thamer C, et al. Interscapular fat is strongly associated with insulin resistance. *J Clin Endocrinol Metab*. 2010;95(10):4736–4742.
21. Matthaei S, et al. Pathophysiology and pharmacological treatment of insulin resistance. *Endocr Rev*. 2000;21(6):585–618.
22. Würslin C, et al. Topography mapping of whole body adipose tissue using A fully automated and standardized procedure. *J Magn Reson Imaging*. 2010;31(2):430–439.
23. Matsuda M, DeFronzo RA. Insulin sensitivity indices obtained from oral glucose tolerance testing: comparison with the euglycemic insulin clamp. *Diabetes Care*. 1999;22(9):1462–1470.

24. Babbar R, et al. Prediction of glucose tolerance without an oral glucose tolerance test. *Front Endocrinol (Lausanne)*. 2018;9:82.
25. Liu FT, et al. Isolation Forest. https://cs.nju.edu.cn/zhouzh/zhouzh.files/publication/icdm08b.pdf?q = isolation-forest. Accessed September 29, 2021.
26. Cambria E, White B. Jumping NLP curves: a review of natural language processing research. *IEEE Computat Intell Mag*. 2014;9:48–57
27. Shrikumar A, et al. Learning Important Features Through Propagating Activation Differences. http://arxiv.org/abs/1704.02685. Accessed September 29, 2021.
28. Clevert D-A, et al. Fast and Accurate Deep Network Learning by Exponential Linear Units (ELUs). https://arxiv.org/abs/1511.07289. Accessed September 29, 2021.
29. He K, et al. Delving Deep into Rectifiers: Surpassing Human-Level Performance on Imagenet Classification. https://arxiv.org/abs/1502.01852. Accessed September 29, 2021.
30. Kingma DP, Ba J. Adam: A Method for Stochastic Optimization. https://arxiv.org/abs/1412.6980. Accessed September 29, 2021.
31. Abadi M, et al. TensorFlow: Large-Scale Machine Learning on Heterogeneous Systems. https://arxiv.org/abs/1603.04467. Accessed September 29, 2021.
32. Nickolls J, et al. Scalable parallel programming with CUDA: is CUDA the parallel programming model that application developers have been waiting for?. *ACM Queue*. 2008;6(2):40–53.

HHS Public Access

Author manuscript

Abdom Radiol (NY). Author manuscript; available in PMC 2025 June 01.

Published in final edited form as:

Abdom Radiol (NY). 2024 June ; 49(6): 2116–2124. doi:10.1007/s00261-024-04310-y.

Cross-sectional imaging of the pancreas in diabetes

John Virostko[1,2,3,4], **Temel Tirkes**[5,6,7]

[1]Department of Diagnostic Medicine, Dell Medical School, University of Texas at Austin, 10 E 24th Street, Austin, TX 78712, USA

[2]Livestrong Cancer Institutes, Dell Medical School, University of Texas at Austin, Austin, TX, USA

[3]Department of Oncology, Dell Medical School, University of Texas at Austin, Austin, TX, USA

[4]Oden Institute for Computational Engineering and Sciences, University of Texas at Austin, Austin, TX, USA

[5]Department of Radiology and Imaging Sciences, Indiana University School of Medicine, Indianapolis, IN, USA

[6]Department of Medicine, Division of Gastroenterology and Hepatology, Indiana University School of Medicine, Indianapolis, IN, USA

[7]Department of Urology, Indiana University School of Medicine, Indianapolis, IN, USA

Abstract

Diabetes mellitus presents a global health challenge characterized by dysregulated glucose metabolism and insulin resistance. Pancreas dysfunction contributes to the development and progression of diabetes. Cross-sectional imaging modalities have provided new insight into the structural and functional alterations of the pancreas in individuals with diabetes. This review summarizes MRI and CT studies that characterize pancreas alterations in both type 1 and type 2 diabetes and discusses future applications of these techniques.

Keywords

Volume; Quantitative; MRI; CT; Fat; Type 1 diabetes; Type 2 diabetes; T1D; T2D

Introduction

As the sole organ capable of insulin production, the pancreas plays a key role in the pathogenesis of both type 1 diabetes (T1D) and type 2 diabetes (T2D). Indeed, the crucial link between the pancreas and diabetes has been known since 1889, when German physicians Oscar Minkowski and Josef von Mering removed the pancreas of a dog. The flies subsequently swarming the dog's urine was an unmistakable sign of sugar in the urine, implicating the role of the pancreas (namely release of the hormone insulin from pancreas

✉John Virostko, jack.virostko@austin.utexas.edu.

islets) in preventing diabetes. Three decades later insulin was purified from the pancreas and a new paradigm of diabetes treatment ensued.

Despite its central role in maintaining glucose homeostasis, the pancreas is not imaged as part of routine diabetes care. Endocrinology relies heavily upon laboratory assays of bodily fluids; in the case of diabetes these consist primarily of glucose and insulin. However, there is growing recognition of the shortcomings of these assays. Measures of insulin secretion following a glucose challenge can induce patient discomfort and are hampered by poor reproducibility [1]. Additionally, the amount of insulin secreted following a glucose challenge provides insight into insulin secretory capacity, but does not necessarily reflect islet mass nor insulin sensitivity [2, 3]. Furthermore, glucose homeostasis is thought to be unaffected until islet mass is reduced by half or more, putatively due to a large functional reserve capacity [4–6]. The small size of pancreatic islets and their scattered distribution throughout the pancreas have made them extremely difficult to image non-invasively in humans [7–9]. However, diabetes is accompanied by alterations to the whole pancreas that are amenable to imaging and may correlate with islet mass and/or other hallmarks of diabetes pathogenesis. In this review, we highlight cross-sectional imaging techniques which detect changes to the pancreas in individuals with diabetes and discuss their possible role in early diagnosis and monitoring of diabetes.

Size and morphology

Prior to imaging, autopsy studies found that the pancreas is markedly smaller in individuals with both T1D [10] and T2D [11]. Several imaging studies have now corroborated these findings across a range of imaging modalities and populations with diabetes, both adult and pediatric. Compellingly, a meta-analysis of imaging studies suggests smaller pancreas size in T1D than T2D [12]. Abdominal MRI from the UK Biobank study similarly found smaller pancreas size in T1D than T2D and identified genome wide associations with pancreas size [13]. Figure 1 shows an abdominal MRI of an individual with and without T1D, demonstrating smaller pancreas size in the individual with diabetes.

The pathophysiology underlying a smaller pancreas size in individuals with diabetes is under investigation. The degree of pancreas reduction in both type T1D and T2D (> 20%) far exceeds the volume of the endocrine pancreas (which comprises only 1–2% of the pancreas), suggesting exocrine involvement in diabetes pathogenesis. Histological studies of the pancreas from T1D donors confirm exocrine involvement, demonstrating reduced numbers of acinar cells [14], altered exocrine cell expression [15], and immune infiltration into the exocrine compartment [16]. The dynamics of pancreas size in relation to the development of diabetes are unclear. For instance, it is not known if the pancreas shrinks due to diabetic insult or if a small pancreas (perhaps due to impaired pancreas development during childhood) imparts risk for developing the disease. The pancreas is smaller in patients with new onset T1D [17–19] as well as in individuals at high risk of developing T1D [20, 21], suggesting that small pancreas size may occur early in the disease process. MRI studies of pancreas diameter [22] and pancreas volume [23] demonstrate increases in pancreas size during childhood and atrophy after middle age. The pancreas also displays dynamic changes in size associated with diabetes. Our longitudinal studies of pancreas volume in patients with

recent-onset T1D found that pancreas volume declines over the first year after diagnosis [21] and continues to decline with longer T1D duration [24]. In patients at risk for developing T1D, pancreas size declines prior to diagnosis with clinical disease [25]. In studies of patients with T2D, remission is accompanied by increases in the size of the pancreas [26]. These findings indicate that pancreas size is dynamic and may be useful for prediction and/or monitoring of diabetes. Studies of patients undergoing pancreatectomy have found that pancreas size correlates with the number of pancreatic islets isolated from each donor organ [27, 28]. Individuals with insulin gene mutations also have smaller pancreas size, implicating intrapancreatic insulin action as a mediator of pancreas size [29]. Taken together, these studies suggest that pancreas size can reflect dynamic changes in pancreatic islet function and/or mass. While MRI can accurately measure pancreas volume and thickness with high reproducibility [30, 31], there are no established pancreatic size criteria adjusted for age and sex that can be applied to clinical practice.

The pancreas is an elongated organ that has been compared in shape to a leaf, banana, pear, and tadpole. The unique shape of the pancreas stems from its embryological origins as the fusion of two distinct buds which form the head of the pancreas and body/tail of the pancreas, respectively. Interestingly, the morphology of the pancreas appears to change in response to pancreatic diseases. For instance, focal pancreatic atrophy can appear at the site of subsequent tumor formation [32]. In patients with T1D, the pancreas thins circumferentially rather than longitudinally, possibly suggesting loss of acinar tissue and preservation of ductal tissue [24]. Patients with T2D also display altered pancreas morphology, with increasingly serrated borders [33] that become normalized after disease remission [26]. Imaging of pancreas shape can provide insight into the focality of diabetic insult and may help us better understand the pathophysiology underlying smaller pancreas size.

Steatosis

Pancreatic fat content can be quantified with high reproducibility by MRI [34] or CT [35]. Figure 2 demonstrates pancreas fat fraction measurements acquired using multi-echo Dixon MRI. Prior studies have reported a higher prevalence of pancreatic fat fraction (i.e., steatosis) in patients with T2D and obesity [36–38]. In contrast, pancreatic fat content does not appear to be altered in T1D [39]. Tirkes et al. reported that patients with T2D had significantly higher pancreatic fat (23%; 95%CI: 21–25%) than non-diabetic individuals (15%; 95%CI:14–17%; $p = 0.03$). His study showed an increase in the probability of diabetes with a higher pancreatic fat fraction [40]. There was also a moderate positive correlation between the pancreatic fat fraction with the amount of visceral and subcutaneous adipose tissue ($r = 0.54$ and $r = 0.23$, respectively). These findings agree with other studies examining the relationship between pancreatic fat and diabetes, most of which showed a positive association between the two conditions [37, 38]. Increased fat content may precede diagnosis with diabetes, as pancreatic fat content is increased in individuals at risk for developing T2D [41–43]. As with pancreas size, pancreatic fat content may exhibit dynamic changes in individuals with diabetes. CT imaging of pancreatic fat showed a correlation between fat content and disease duration that correlates with measures of glycemic control [44]. Conversely, diet-induced reversal of T2D was accompanied by a

decline in pancreatic fat fraction [45]. The metabolic and clinical implications of pancreatic steatosis are uncertain. MRI studies of individuals with T2D have demonstrated higher pancreatic fat associated with reduced insulin secretion [46, 47]. Moreover, pancreatic fat was positively associated with risk of developing pancreatic cancer [48]. Comparative studies of chemical shift-based methods for pancreas fat quantification indicated good agreement [49]. Additionally, MRI and CT-based measurement of pancreas fat correlate [50]. Both MRI and CT methods for quantifying pancreatic fat content are common on clinical scanners and relatively straightforward to implement.

Magnetic resonance relaxometry

The T1 relaxation time, which measures how fast the nuclear spin magnetization returns to its equilibrium state after a radiofrequency pulse in the MRI scanner, is a crucial source of soft tissue contrast in MRI. The healthy pancreas has a shorter T1 relaxation time than any other abdominal organ due to the protein-rich cytoplasm of acinar cells [51]. This tissue property translates into a hyperintense (bright) signal on fat-suppressed unenhanced T1-weighted imaging [51]. It has been postulated that patients with T1D exhibit exocrine pancreas dysfunction secondary to lack of insulin and dys-regulation of endocrine function [52]. An estimated 25–75% of adult patients with T1D have concomitant exocrine pancreas insufficiency (EPI). The hyperintense T1 signal of the pancreas has been shown to decrease in the presence of EPI as the acinar cells are reduced [53], a finding that has been confirmed with histopathology [54, 55]. Tirkes et al. correlated T1 signal intensity ratio of the pancreas with EPI, which was determined via pancreatic function testing that endoscopically collects pancreatic fluid for analysis. His study showed a significant direct correlation between the pancreatic fluid bicarbonate level and the T1 signal intensity ratio ($r = 0.70$, $p < 0.0001$) [56]. This study also showed that T1 signal intensity ratio is more sensitive at detecting EPI than the volume of pancreatic fluid excreted into the duodenum in response to secretin stimulation. T1 maps, in which the pixel values represent the T1 relaxation time depict relatively small variations to highlight tissue pathology (Fig. 3). Tirkes et al. compared different T1 mapping techniques to determine the ideal MR imaging technique for the pancreas and liver [57, 58]. He was also the first investigator to report the average T1 relaxation times in patients with chronic pancreatitis (CP) and non-diseased pancreas [59]. Noda et al. reported that pancreatic T1 relaxation time is significantly increased in pre-diabetic individuals and moderately correlates with HbA1c, suggesting that T1 has the potential of being a predictive biomarker for diabetes [60]. More studies are needed to confirm these findings and to monitor longitudinal changes in T1 relaxation time associated with diabetes.

Extracellular volume fraction (ECV) is a quantitative measurement of the T1 relaxation time derived before and after administering MRI contrast agent. ECV is commonly measured in myocardial imaging to dichotomize tissues between intracellular and extracellular spaces [59, 61]. Prior studies have implicated pancreatic islet dysfunction/apoptosis and diabetes secondary to islet amyloid deposition, which can be detected by higher ECV fraction [62–65]. Noda et al. recently reported positive correlations of HbA1c with both pre-contrast pancreatic T1 relaxation time ($r = 0.79$, $p < 0.001$) and ECV fraction ($r = 0.60$, $p < 0.001$) [66]. Pre-contrast pancreatic T1 relaxation time and ECV fractions were significantly

higher in individuals with diabetes than those with pre-diabetes or no diabetes ($p < 0.001$). Measurement of T1 has traditionally required sophisticated image analysis, but modern MR scanners are increasingly adding this capability as an optional package.

Diffusion-weighted imaging

Diffusion-weighted MRI can detect alterations in the random motion of water molecules within biological tissue that are indicative of disease. Accordingly, diffusion can detect changes in cell density, membrane integrity, and inflammation within the pancreas. Water diffusion in biological tissue is commonly quantified using the apparent diffusion coefficient (ADC) which quantifies the magnitude of water motion over a short time scale. A higher ADC signifies less constrained water motion and is often indicative of inflamed tissue while a lower ADC can signify fibrotic tissue. Pancreas diffusion is known to be altered in individuals with pancreatitis and pancreatic cancer, with lower ADC in both diseases [67]. When applied to study diabetes, ADC was found to be higher in individuals with fulminant T1D and correlated with disease duration and glycemic control [68]. Our own work did not detect differences in the ADC of individuals with T1D when measurements were averaged throughout the pancreas [21]. However, using histogram analysis we found an increased number of voxels with high ADC values in the pancreas of individuals with T1D, suggesting focal regions of inflammation in the pancreas. Figure 4 displays example ADC maps for an individual with T1D and one without diabetes. In individuals at risk for T2D, a negative correlation was found between pancreatic ADC and HbA1c [69]. This same study also calculated diffusion kurtosis by acquiring diffusion weighted-imaging with more strongly diffusion-weighted images (higher ‘b-values’) and fitting data to a model incorporating non-Gaussian Brownian motion. Diffusion kurtosis was found to correlate with HbA1c, with higher kurtosis in the group with highest HbA1c [69]. Diffusion-weighted imaging has the benefit of being widely used on clinical MRI scanners and its repeatability and reproducibility are well characterized.

Perfusion imaging

The islets of Langerhans receive a disproportionate share of pancreatic perfusion (10–20%) given their relatively minor contribution to total pancreatic volume (1–2%) [70]. Glucose is a potent stimulant for islet cell perfusion, increasing blood flow by up to 3-fold [71, 72]. The mechanism for glucose regulation of pancreatic islet blood flow is not entirely understood [71]. Given the relatively high blood flow to islets and their response to glucose stimulation, there have been numerous attempts to image pancreas perfusion. A recent study investigated pancreatic perfusion and its response to glucose stimulation in patients with T1D by dynamic positron emission tomography utilizing ^{15}O-labelled water. Patients with T1D showed a 23% lower baseline pancreatic perfusion than non-diabetic controls ($p = 0.0497$) [73]. After intravenous glucose administration, total pancreatic perfusion increased by 48% in controls but not in individuals with diabetes, suggesting that both basal and stimulated islet perfusion is perturbed in those with diabetes. One hypothesis is that pancreatic perfusion is compromised by acute pancreatitis leading to islet cell hypoperfusion and diabetes [74, 75]. MRI approaches for imaging pancreas perfusion have included arterial spin labeling (ASL), intravoxel incoherent motion (IVIM), and dynamic contrast enhanced

magnetic resonance imaging (DCE-MRI). ASL of the pancreas has measured increased pancreas perfusion in response to a glucose bolus [76], as shown in Fig. 5. ASL studies of diabetic patients have been relatively limited, but ASL performed during hyperglycemic clamp did not detect a difference between individuals with T1D and controls [75]. IVIM refers to the random microscopic motion that occurs within voxels on MR images of water molecules (either intracellular or extracellular) and the microcirculation of blood [77]. While IVIM studies of individuals with diabetes are lacking, IVIM has demonstrated correlation with glucose stimulated pancreas perfusion increases in porcine models [78]. Dynamic contrast enhanced magnetic resonance imaging (DCE-MRI) is the acquisition of sequential images during the passage of a contrast agent through a tissue of interest. A study of DCE-MRI in individuals with T2D found increased vascular permeability in the pancreas, and that perfusion changes correlated with disease duration [79]. MRI has demonstrated the ability to measure changes in pancreas perfusion in response to glucose using several different approaches, but these studies are relatively limited. Comparison studies between perfusion imaging techniques are needed to cross-validate these approaches.

Magentic resonance elastography

Magnetic resonance elastography (MRE) can be used to noninvasively estimate the stiffness of soft tissues. MRE relies on imaging tissue exposed to high frequency vibrations, which tend to move slower in stiff tissues. An example map of pancreas stiffness generated by MRI is shown in Fig. 6. Test-retest studies have demonstrated that MRE of the pancreas is repeatable in individuals at one-month intervals [80]. MRE has detected increased stiffness in the pancreas of patients with chronic pancreatitis [81]. Individuals with diabetes have also been found to have higher pancreas stiffness than controls using MRE [82]. The basis for this increased stiffness is putatively fibrosis and acinar atrophy, both of which have been linked to MRE-derived stiffness in histological studies [83]. Interestingly, MRE may be sensitive to the dynamics of pancreatic glucose metabolism, as injection of a glucose bolus led to pancreas stiffening [84]. This glucose-induced stiffening may be related to changes in pancreas perfusion, as detailed in the prior section. Although primarily a research tool at present due to its complexity, the role of MRE in abdominal imaging is likely to grow with future vendor support for imaging hardware and software.

Radiomics

Given their ability to image the entire pancreatic volume, cross-sectional imaging techniques such as CT and MRI can be used to detect spatial heterogeneity throughout the pancreas. Figures 2, 3, 4, 5 and 6 demonstrate spatial heterogeneity throughout the pancreas for a variety of tissue properties. Indeed, the pancreas is a complex structure encompassing not only the endocrine islets, but also the acinar cells and ductal network comprising the exocrine component of the gland. There are differences in the relative concentration of these components across the pancreas, with higher relative numbers of islet in the pancreas tail than the pancreas head [85]. Autopsy studies of the pancreas from donors with diabetes demonstrate spatial heterogeneity in the disease process. In T1D, there is marked lobular heterogeneity in the autoimmune infiltrate characteristic of T1D [86]. In T2D, the islet amyloids and corresponding exocrine fibrosis are heterogeneous throughout the pancreas

[87, 88]. While our current understanding of the spatial patterns of diabetic insult to the pancreas is limited, imaging can play a key role in mapping regional pathophysiology. Unlike histological measurements, which are subject to sampling bias and can be difficult to reconstruct for the entire organ, cross-sectional images of the pancreas form an atlas of the whole organ. Moreover, the burgeoning field of radiomics can provide tools for identifying and quantifying spatial heterogeneity. Radiomics combines high throughput feature extraction from quantitative imaging data with multidimensional texture, histogram, shape, and wavelet analysis [89]. While its application to pancreas imaging in individuals with diabetes is currently limited, radiomics holds great promise for characterizing and quantifying the spatial heterogeneity of the diabetic pancreas. For example, histogram analysis of the pancreas of individuals with T1D identifies areas within the pancreas with altered diffusion that are not evident when averaging the signal across the whole pancreas [21]. This finding highlights the spatial heterogeneity of the diabetic process in the pancreas and the need for radiomic analysis to detect focal changes.

Conclusion

Cross-sectional MRI and CT have identified differences in the size, structure, and composition of the pancreas of individuals with diabetes. Further application of these imaging techniques may improve our understanding of the pathogenesis of diabetes, facilitate its early diagnosis, and enable monitoring of therapeutic interventions. Imaging endpoints may speed clinical trials of novel diabetes therapies, as the metabolic endpoints currently employed are often inadequate surrogate markers and can require lengthy monitoring periods. Imaging the pancreas may better help us understand differences between T1D and T2D, which are increasingly being thought of as a spectrum of disease, rather than a dichotomy [90]. Furthermore, imaging-based pancreas phenotyping may improve our understanding of other ‘atypical’ forms of diabetes [91] and their relationship with more classical models of T1D and T2D. While imaging will never replace the laboratory tests that form the backbone of diabetes diagnosis and management, it can play a vital role in diabetes care and interrogate aspects of the disease not captured by measures of glucose and insulin.

Acknowledgements

Research reported in this publication was supported by the Beatson Foundation (2021-003), National Institute of Diabetes and Digestive and Kidney Diseases (DK129979, DK097771, DK108323, DK127382), and the National Cancer Institute (CA260955). Funding was provided via the NIDDK Information Network New Investigator Pilot Program in Bioinformatics. We gratefully acknowledge contributions from the Consortium for the Study of Chronic Pancreatitis, Diabetes, and Pancreatic Cancer (CPDPC) and Imaging Morphology of Pancreas in Diabetic Patients following Acute Pancreatitis (IMMINENT) Study.

References

1. Hudak S, et al. , Reproducibility and discrimination of different indices of insulin sensitivity and insulin secretion. PLoS One, 2021. 16(10): p. e0258476. [PubMed: 34679116]
2. McCulloch DK, et al. , Correlations of in vivo beta-cell function tests with beta-cell mass and pancreatic insulin content in streptozocin-administered baboons. Diabetes, 1991. 40(6): p. 673–9. [PubMed: 2040383]
3. Robertson RP, Estimation of beta-cell mass by metabolic tests: necessary, but how sufficient? Diabetes, 2007. 56(10): p. 2420–4. [PubMed: 17606873]

Key points

Cross-sectional imaging can detect alterations to the pancreas accompanying, and possibly presaging, the development of both type 1 diabetes (T1D) and type 2 diabetes (T2D).

The smaller pancreas found in individuals with diabetes implicates exocrine involvement in the disease, as it exceeds the 1–2% of the pancreas composed of hormone-producing endocrine tissue.

Pancreas fat content is associated with insulin resistance and is higher in individuals with T2D.

Quantitative MRI can detect changes in pancreas composition and microstructure in individuals with diabetes that display spatial heterogeneity throughout the gland.

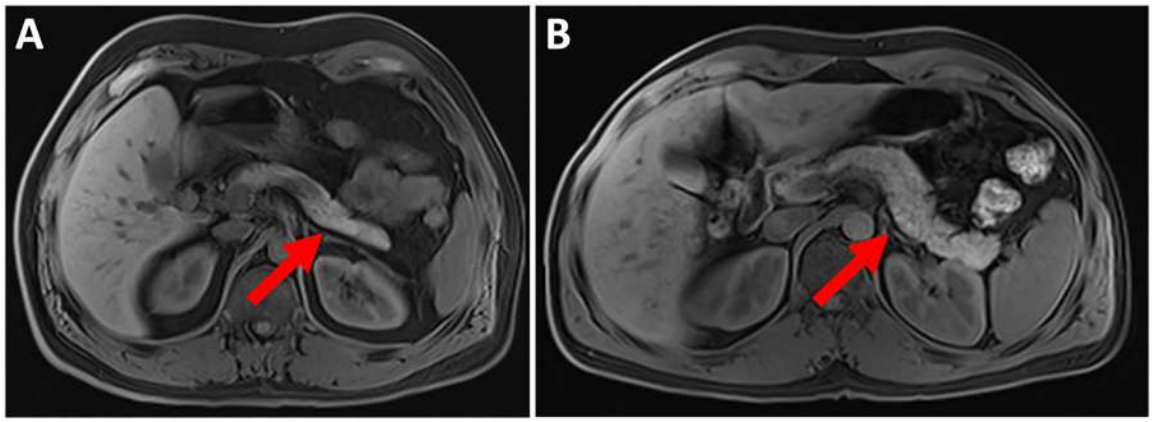

Fig. 1.

Axial slices from an unenhanced, T1-weighted abdominal 3T MRI of (**A**) a 53-year-old male with T1D duration of 51 years and (**B**) a 29-year-old male without diabetes demonstrates a smaller pancreas in the individual with T1D. The red arrow marks the pancreas on similar slices for each study participant. Note the dramatic circumferential shrinking of the pancreas in the participant with T1D.

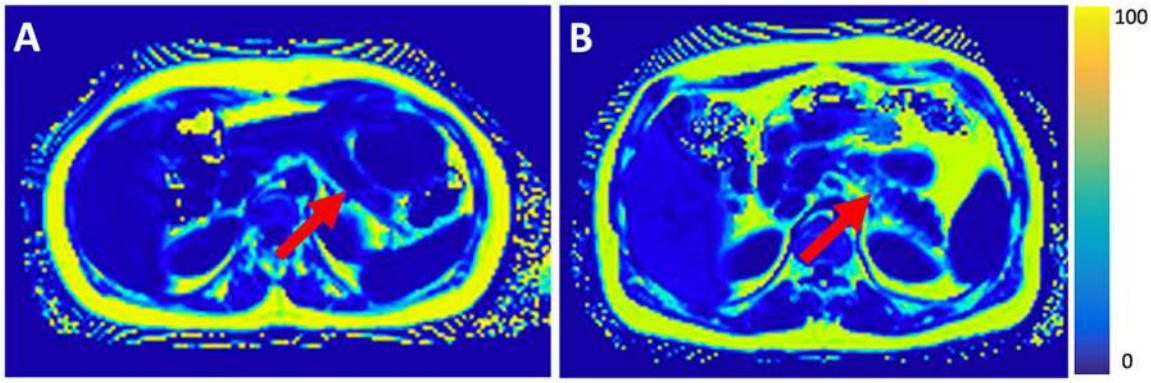

Fig. 2.

Quantitative fat fraction map derived from multi-echo Dixon MRI of (**A**) a 33-year-old female with limited pancreatic steatosis (average = 7.9%) and (**B**) a 41-year-old male with significant pancreatic steatosis (average = 23.9%). On both images the location of the pancreas is indicated on axial slices by a red arrow. The colorbar displays the fat fraction in pseudocolor.

Fig. 3.
Unenhanced axial T1 relaxation time map of a 42-year-old female patient. White arrows indicate the body of the pancreas.

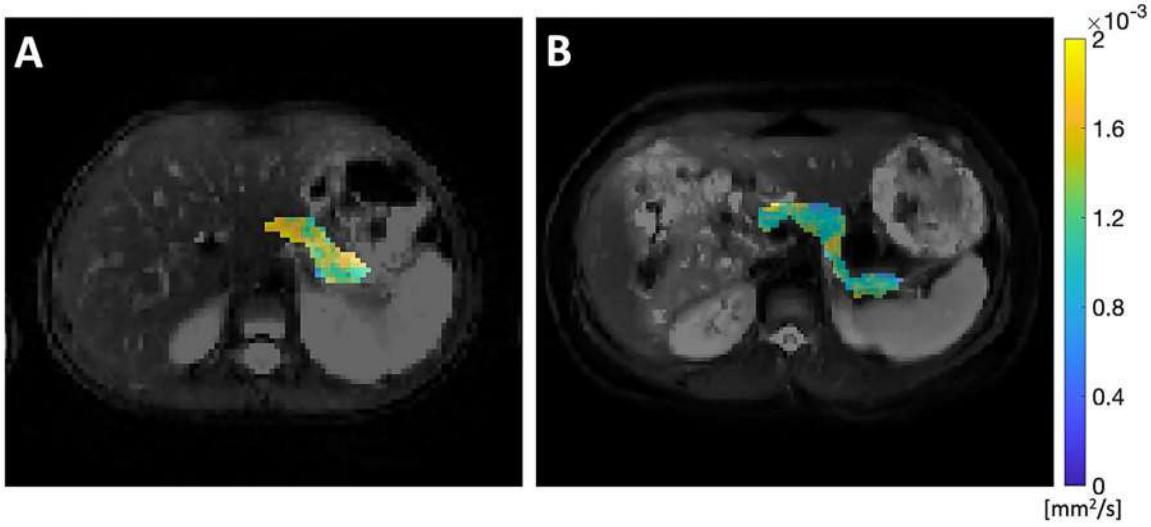

Fig. 4.

A) An 8-year-old boy with recent onset T1D displays a higher apparent diffusion coefficient (ADC) in the pancreas than **B**) a 9-year-old boy without diabetes. Apparent diffusion coefficient values are displayed in pseudo color throughout the pancreas and overlaid over a T2-weighted axial image.

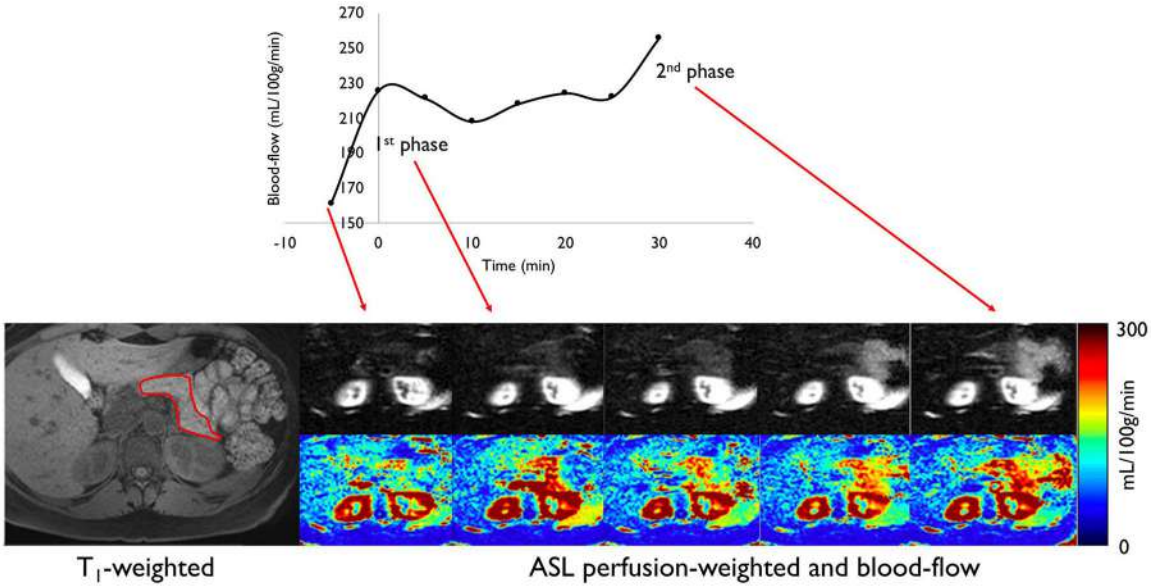

Fig. 5.

Arterial spin label-based imaging of pancreas perfusion demonstrates a biphasic increase in blood flow in response to oral glucose stimulation. The bottom row displays axial maps of pancreas perfusion at serial time points after ingestion of glucose. Figure adapted from reference [76] with permission, © 2020 John Wiley & Sons, Inc

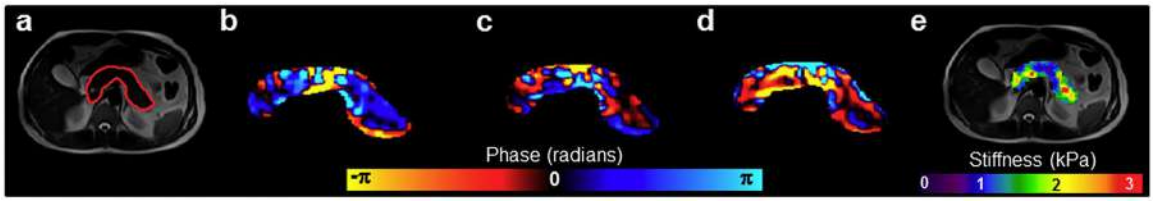

Fig. 6.

Example magnetic resonance elastography images of the pancreas including: (**a**) Magnitude image with red contour delineating the pancreas, (**b**–**d**) snapshot of curl displacement field in the three spatial encoding directions (i.e., x, y, z), respectively, and (**e**) the corresponding overall weighted stiffness map. Figure adapted from reference [80] with permission, © 2017 Elsevier

Identifying diabetic eye disease

Eye diseases related to diabetes include a range of conditions such as refractive changes, double vision, cataract, glaucoma and diabetic retinopathy. Of these conditions, diabetic retinopathy is the only one that is directly caused by diabetes and that most frequently results in vision loss.

An eye condition that is caused by diabetes – diabetic retinopathy

Diabetic retinopathy results from damage to the small blood vessels of the retina through changes in the blood flow. Initially diabetic retinopathy may cause few or mild symptoms but, as the disease progresses, it can lead to blindness. Diabetic retinopathy can cause changes in the eye including:

- Microaneurysms – small bulges in the blood vessels of the retina that can leak fluid into the retina
- Retinal haemorrhages – tiny spots of blood that leak into the retina
- Hard exudates – lipid deposits
- Cotton wool spots – swollen ischaemic axons in the nerve fibre layer
- Venous dilation and beading
- Intraretinal microvascular abnormalities – abnormal branching or dilation of existing blood vessels
- Abnormal new vessels – depending on the location of the new vessels, these are classified as either "neovascularisation of the disc" or "neovascularisation elsewhere"

(See Appendix 1 for examples of retinal photographs)

Non-proliferative diabetic retinopathy

The early stage of diabetic retinopathy is known as "non-proliferative diabetic retinopathy". During this stage the microvascular abnormalities are limited to the retina.

Proliferative diabetic retinopathy

Proliferative diabetic retinopathy occurs as a result of microvascular abnormalities that restrict blood flow to the retina which deprives it of oxygen. In an attempt to supply blood to the deprived areas, new blood vessels grow from the retina into the vitreous cavity.

Proliferative diabetic retinopathy can cause severe vision loss via vitreous

Normal retina

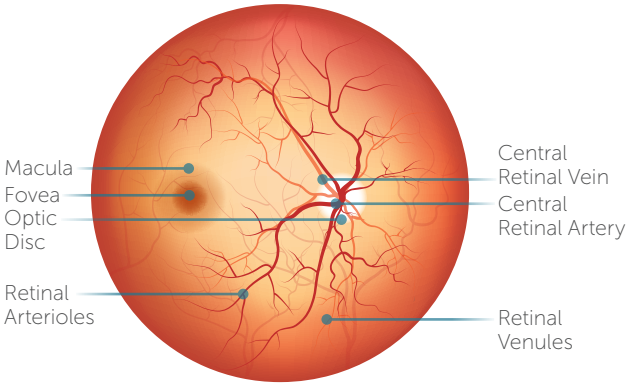

Diabetic retinopathy

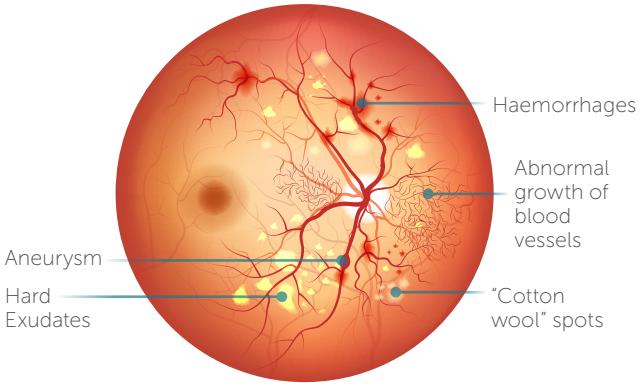

haemorrhage, tractional retinal detachment and neovascular glaucoma.

Diabetic macular edema

Diabetic maculopathy affects the central part of the retina—the macula— which is important for central vision. This may be through lack of blood flow or swelling and the most common form is diabetic macular edema (DME).

In clinical practice the presence and severity of DME is assessed and documented separately from the stage of diabetic retinopathy. DME is potentially sight threatening. If there are signs of DME particularly involving the centre of the macula, the patient should be seen as soon as possible by an ophthalmologist.

Eye conditions that may be exacerbated by diabetes

These eye conditions are not caused by diabetes but are more prevalent and, in some cases, deteriorate faster in people with diabetes. While these conditions are less likely to cause vision loss they are still of concern and should be kept in mind by primary health professionals.

Refractive changes

Variations in blood glucose levels may cause changes in the refractive power of the eye. If a person presents to an eye care practitioner with substantial refractive changes, this may indicate substantial changes in the level of blood glucose.

Diplopia

Diplopia (double vision) is the simultaneous perception of two images of a single object that is caused by damage to the nerves that control eye movement coordination. Diabetes is the leading cause of the nerve damage that disrupts normal eye movement.

Cataract

Cataracts are characterised by clouding of the lens that affects vision and can appear in one or both eyes. Snowflake cataracts with white opacities may affect people with type 1 diabetes and sub-optimal metabolic control. Age-related cataract tends to occur earlier among people with diabetes than people without diabetes[8].

Glaucoma

Glaucoma is a group of progressive conditions that results in damage to the optic nerve. It usually occurs when fluid builds up in the front part of the eye. Glaucoma can permanently damage vision in the affected eye(s), reducing peripheral vision and resulting in irreversible visual loss.

- Open-angle chronic glaucoma develops slowly over time and often is asymptomatic until the disease has progressed significantly
- Closed-angle glaucoma is characterised by sudden eye pain and other symptoms, and is treated as a medical emergency
- Neovascular glaucoma can be seen in advanced cases of proliferative diabetic retinopathy.

Clinical Tip: Key risks

All people with diabetes are at risk of developing retinopathy.

The major risk factors for developing and progression of retinopathy are:

- The duration of diabetes
- High glucose levels
- High blood pressure

Different types of diabetes and implications for eye health

There are three common types of diabetes: type 1, type 2 and gestational diabetes.

Type 1 diabetes is a chronic autoimmune disease in which the immune system destroys the insulin-producing cells in the pancreas. People with type 1 diabetes need lifelong treatment with insulin on a daily basis to control blood glucose. The onset of type 1 diabetes is common in children and young adults but can affect people of any age.

Type 2 diabetes accounts for most cases of diabetes and is characterised by insulin resistance and insufficient insulin production. Type 2 diabetes can often be controlled through diet, weight loss where necessary and increased physical activity. It can also require treatment with medication, including insulin. Type 2 diabetes usually occurs in adults but is increasingly seen in children and adolescents.

Many people live with type 2 diabetes for long periods without recognising symptoms or being aware of their condition. By the time of diagnosis, their organs may already be damaged by excess blood glucose and complications such as retinopathy may already be evident.

Gestational diabetes develops during pregnancy and usually resolves after the woman gives birth. Women who have gestational diabetes remain at significant risk of developing type 2 diabetes later in life.

Ophthalmic staff preparing to see patients, Ethiopia. Photo: Lance Bellers/Sight Savers. CC BY-NC 2.0 CEHJ

Strategies to managing eye health

It is important that all people with diabetes are routinely screened for diabetic retinopathy in order to prevent progression and development of diabetes-related loss of vision. Duration of diabetes is a major risk factor associated with the development of diabetic retinopathy. Regular eye examinations are the only way to determine the extent of diabetic retinopathy: the patient may not yet be experiencing any vision loss as the early stages of retinopathy are asymptomatic.

Strategies used by health professionals to support people with diabetes include:

- Clearly communicate to the person with diabetes the need for ongoing eye exams over their lifetime
- Encourage lifestyle modification; give individually tailored diabetes-specific advice about physical activity and nutrition
- Develop individual plans that suit each person's needs and are appropriate to resources available
- Provide support for ongoing self-management
- Ensure regular contact with health professionals and supportive peers
- Ensure access to education programmes, including education on eye health.

Table 1 Timing of initial and ongoing eye examinations for people with diabetes

Eye Examination	Type 1 diabetes	Type 2 diabetes	Gestational diabetes
Initial examination	Initiate within five years after the diagnosis of diabetes If date of onset unknown, assume that the duration of diabetes is more than five years Children: five years after diagnosis or at puberty, whichever is the earlier	Initiate as soon as possible after diagnosis of diabetes	Conduct on diagnosis of gestational diabetes
Ongoing examinations	Conduct regular examination every one to two years if no abnormality is detected Once retinopathy is detected, frequency of assessments may need to increase depending on severity of the retinopathy and level of control of systemic risk factors. (See Table 5 *Referral criteria for people with type 1 diabetes and type 2 diabetes*)		No need for further examination if diabetes resolves after delivery

Detection of diabetic retinopathy

Screening should be undertaken by any suitably trained practitioner. Often it is not practical, or an effective use of resources, to have every person with diabetes screened by a specialised eye physician such as ophthalmologist or retinal specialist. Retinal screening for diabetic retinopathy and its severity can be performed by a person (who may not have a medical degree) if they have been properly trained to perform ophthalmoscopy or retinal photography.

In a primary care or non-speciality setting, eye examinations for detecting diabetic retinopathy can be carried out using a fundus camera to take retinal photographs. This requires a specifically designed digital camera to take images of the eye. The camera is not complicated and operators do not require advanced training. The images are either read locally or sent electronically to a central facility for reading[10].

If no major eye problems are detected then regular visual acuity testing and retinal examination is recommended.

Clinical Tip: Eye examination at diagnosis

Ideally, at the time of diagnosis of diabetes, a person should have a comprehensive eye examination alongside an assessment of the extent to which diabetes-related complications have already occurred.

Regular eye examinations should then be repeated over the person's lifetime.

Eye examination

Ideally, examination methods should be identical in different settings and the same sequence should be followed in both low-resource and resource-rich settings. As a minimum, managing eye health in people with diabetes should include:

1. Medical history
2. Eye screening (see Table 2)
    a. Visual acuity test
    b. Retinal examination adequate for diabetic retinopathy classification which would generally involve each retina being closely inspected for signs of diabetic eye disease using one of the methods below

The method used for retinal examinations will depend on the resources available and the level of training of the practitioner. The health practitioner's role is central; either to perform the screening or to check that it is occurring regularly. Some form of patient recall system is a valuable tool to remind both practitioners and patients about the need for regular fundus screening.

A checklist for conducting a medical history and eye examination is provided at Appendix 1.

Table 2 Eye screening for people with diabetes

Visual acuity (test prior to pupil dilation)	
Refraction and visual acuity assessment with a visual acuity lane and a high-contrast visual acuity chart	
Or	
Near or distance eye chart and a pin-hole option to see if visual acuity is reduced	
Retinal examination	
Non-mydriatic retinal photography	Recommended as a screening method Provides a permanent record Dilated pupils may improve sensitivity and image quality Can be carried out using telemedicine
Or	
Binocular indirect ophthalmoscopy	Pupils must be dilated Large field view Can be combined with slit-lamp examination to examine peripheral retina
Or	
Mydriatic retinal photography (conventional fundus camera)	Pupils must be dilated Provides a permanent record Sensitive method Can be carried out using telemedicine
Or	
Slit-lamp biomicroscopy	Used in routine clinical practice Pupils must be dilated for fundus examination Evaluation of the anterior and posterior segment with contact/ noncontact lenses

Clinical Tip: Pupil dilation

Pupil dilation may improve the sensitivity and image quality, especially when the ocular media are not clear due to cataract.

Grading of diabetic retinopathy and macular edema

The stages of diabetic retinopathy are classified in Table 3 using the International Classification of DR Scale. The retinal examination will indicate the most appropriate course of management.

Diabetic macular edema (DME) is complication of diabetic retinopathy and the presence and severity of DME should be assessed separately to that of diabetic retinopathy (see Table 4). DME can be associated with any of the stages of diabetic retinopathy.

Referral criteria

Approximately one third of people with diabetes will have diabetic retinopathy and approximately one third of those will have a form of diabetic retinopathy that threatens their vision and requires treatment. Timely referral is crucial to ensure early intervention. The recommendations in Table 5 should be tailored for individuals according to their risks for the progression of diabetic retinopathy.

Mobile unit, India. Photo: Project Nayantara. CC BY-NC 2.0 CEHJ

Table 3 Classification of diabetic retinopathy

Diabetic retinopathy (DR)	Findings
No apparent DR	No abnormalities
Mild non-proliferative DR	Microaneurysms only
Moderate non-proliferative DR	More than just microaneurysms but less than severe non-proliferative DR
Severe non-proliferative DR	Any of the following: Intraretinal haemorrhages (≥20 in each quadrant) Definite venous beading (in two quadrants) Intra-retinal microvascular abnormalities (in one quadrant) No signs of proliferative DR
Proliferative DR	Severe non-proliferative DR and one or more of the following: Neovascularisation Vitreous/pre-retinal haemorrhage

Adapted from ICO Guidelines for Diabetic Eye Care[11]

Table 4 Grading of diabetic macular edema

Diabetic Macular Edema	Findings observable on dilated ophthalmoscopy*
DME absent	No retinal thickening or hard exudates in posterior pole
DME present	Retinal thickening or hard exudates in posterior pole
Mild DME	Retinal thickening or hard exudates in posterior pole but outside central subfield of the macula (diameter 1000 µm)
Moderate DME	Retinal thickening or hard exudates within the central subfield of the macula but not involving the centre point – also known as "centre-threatening DME"
Severe DME	Retinal thickening or hard exudates involving the centre of the macula—also known as "DME with centre involvement" or "centre-involved DME"

*Hard exudates are a sign of current or previous macular edema. DME is defined as retinal thickening; this requires a three-dimensional assessment that is best performed by a dilated examination using slit-lamp biomicroscopy and/or stereo fundus photography. Optical coherence tomography is the most sensitive method to identify the sites and severity of DME

Adapted from ICO Guidelines for Diabetic Eye Care[11]

Table 5 Referral criteria for people with type 1 diabetes and type 2 diabetes

Condition	Urgent referral as soon as possible	Referral within four months	Referral within six months	No referral	Repeat examination within one year	Repeat examination in one to two years
Sudden severe vision loss	●					
Retinal tear and/or detachment	●					
Proliferative diabetic retinopathy	●					
Severe DME	●					
Unexplained gradual worsening of vision		●				
Visual acuity below 6/12 (20/40)		●				
Symptomatic vision complaints		●				
Unexplained retinal findings		●				
Visual acuity cannot be obtained		●				
Retinal examination cannot be obtained		●				
Previous laser or anti-VEGF treatment		●				
Glaucoma		●				
Cataract		●				
Inability to visualise fundus		●				
Severe non-proliferative diabetic retinopathy		●				
DME without centre involvement		●				
Moderate non-proliferative diabetic retinopathy (no DME)			●			
Mild non-proliferative diabetic retinopathy				●	●	
No apparent diabetic retinopathy				●		●

Appendix 1

Checklist for managing eye health in people with diabetes

Medical history

- Duration of diabetes
- Past glycaemic control (HbA1c if possible)
- Medications – especially insulin, blood glucose-lowering medication, antihypertensives and lipid-lowering drugs
- Systemic history – renal disease, systemic hypertension, serum lipid levels and pregnancy
- Ocular history and current visual symptoms

Eye screening

a. Visual acuity test: using acuity lane and a high-contrast visual acuity chart. Alternatively, a near or distance eye chart and a pin-hole option to see if visual acuity is reduced. If visual acuity below 6/12 (20/40), refer to eye specialist

b. Retinal examination adequate for diabetic retinopathy classification (see next page)

Actions

- Referral to eye specialist if required
- Other points to discuss with the patient and their carer
  - Discuss management of patient's blood glucose, blood pressure and blood lipids
  - Discuss dietary and lifestyle changes and identify support, if available

Retinal photographs

Red Signs

- Venous beading (v)
- Haemorrhages (h)
- Microaneurysms (not shown)
- New blood vessels (not shown)
- Intraretinal microvascular abnormalities (not shown)
- Vitreous haemorrhage (not shown)

White Signs

- Cotton wool spots (w)
- Hard exudates (e)

For more examples of retinal photographs, see: ICO Guidelines for Diabetic Eye Care[11]

Normal retina

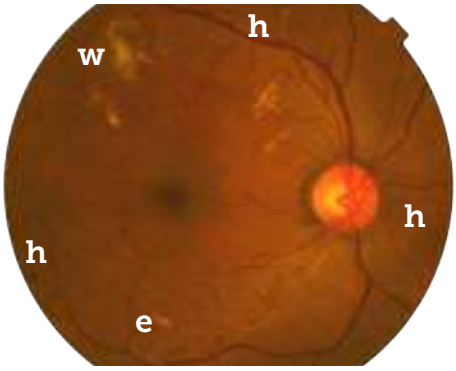

Moderate non-proliferative diabetic retinopathy

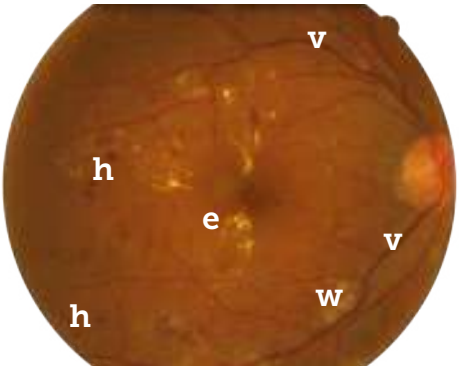

Severe non-proliferative diabetic retinopathy with severe diabetic macular edema

World Health Organization
REGIONAL OFFICE FOR Europe

Diabetic retinopathy screening: a short guide

Increase effectiveness, maximize benefits and minimize harm

Abstract

This guide is designed for policy-makers, public health leaders and senior clinicians involved in planning, designing and implementing diabetic retinopathy screening programmes in the WHO European Region. The purpose of screening is to identify people with diabetes who are at higher risk of developing sight-threatening diabetic retinopathy so that early treatment or intervention can be offered to reduce the incidence of vision impairment or blindness. It demonstrates how the Wilson & Jungner principles apply to diabetic retinopathy screening, describes the pathway to follow and explains how to initiate new programmes or improve the effectiveness of those already existing. The guide forms part of WHO's efforts to increase the effectiveness of screening programmes within the Region, maximizing benefits and minimizing harm.

ISBN 9789289055321

Suggested citation. Diabetic retinopathy screening: a short guide. Increase effectiveness, maximize benefits and minimize harm. Copenhagen: WHO Regional Office for Europe; 2020. Licence: **CC BY-NC-SA 3.0 IGO.**

Cataloguing-in-Publication (CIP) data. CIP data are available at **http://apps.who.int/iris/**

Design: Charlotte Allen.

World Health Organization
REGIONAL OFFICE FOR Europe

CORRIGENDUM

Diabetic retinopathy screening: a short guide. Increase effectiveness, maximize benefits and minimize harm.

ISBN: 97-892-890-5532-1

Subtitle of the publication has been added on the cover page and in suggested citation: Increase effectiveness, maximize benefits and minimize harm.

These corrections were incorporated into the electronic file on 2 July 2021.

Foreword

Diabetic retinopathy is a leading cause of preventable blindness and vision impairment. This guide comes at an important time in the WHO European Region, as trends for diabetes continue to rise and gaps in quality care persist.

The guide aims to capture the challenges policy-makers may face in implementing effective diabetic retinopathy screening and lays out the important steps that should be considered for developing more systematic and quality-assured approaches.

The guide is an output of a cross-programmatic initiative of the WHO Regional Office for Europe that aims to improve screening practices through the life-course and thereby increase effectiveness, maximize benefits and minimize harm. Diabetic retinopathy screening is one of the effective measures recommended by WHO for the prevention and control of noncommunicable diseases, and the prevention of vision impairment and blindness. Combining efforts for better diabetes care and eye care requires ministries of health and public health leaders to work with different stakeholders across professional groups and with patients and at different levels of government. This approach is central to the vision of WHO's European Programme of Work 2020–2025 "United Action for Better Health" for meeting citizens' expectations for health.

We look forward to working with countries to improve the quality of this screening programme, and ultimately improve the quality of life of people with diabetes. We hope this guide proves to be useful in this endeavour.

Jill Farrington
Coordinator, Noncommunicable Diseases

Nino Berdzuli
Director, Division of Country Health Programmes
WHO Regional Office for Europe

Acronyms

ETDRS	Early Treatment Diabetic Retinopathy Study
ICO	International Council of Ophthalmology
NPDR	nonproliferative diabetic retinopathy
OCT	optical coherence tomography
PDR	proliferative diabetic retinopathy
TADDS	Tool for the assessment of diabetic retinopathy and diabetes management systems
VEGF	vascular endothelial growth factor

Executive summary

Diabetic retinopathy is a leading cause of preventable vision impairment and blindness in the WHO European Region (Flaxman et al., 2017). It occurs in about a third of people with diabetes and its damaging effects on vision can be prevented by early detection and treatment through screening (Lee et al., 2015; Thomas et al., 2019; Williams et al., 2004). Vision impairment and blindness have major economic consequences in terms of use of health and social care resources and impact on economic productivity (WHO, 2019).

Although many countries in the WHO European Region have some form of eye checks in place for people with diabetes, these are often not adequately resourced or organized systematically as a screening pathway. Many people with diabetes are living with preventable vision impairment and blindness.

Diabetic retinopathy mainly is caused by the effect of raised blood glucose on the blood vessels in the retina. It can be prevented, and its progression slowed, by control of blood glucose, blood pressure and elevated lipids. If it progresses to an advanced form, treatment with laser and, if available, intraocular drug injections can prevent vision impairment and blindness.

Diabetic retinopathy screening can identify early changes in the retina so treatment can be given before vision impairment or blindness occurs.

The focus of this guide is to show how countries can improve their approach to diabetic retinopathy screening by understanding how to design an effective systematic screening programme.

The guide demonstrates how the principles of screening laid out by Wilson & Jungner (1968) can be applied to screening for diabetic retinopathy. It describes the epidemiology of diabetic retinopathy, how diabetic retinopathy is classified, and considers some of the important design features of a systematic diabetic retinopathy screening programme.

The guide moves on to describe the steps of the screening pathway: identifying the population eligible for screening; invitation and information; testing; referral of screen positives and reporting of screen-negative results; diagnosis; intervention, treatment and follow-up; and reporting of outcomes. It shows that for diabetic retinopathy screening to be most effective, a screening pathway encompassing all these steps should be in place.

The chapters in the guide illustrate how countries can improve the effectiveness of their screening. They provide a framework for undertaking a situational analysis that looks at four domains: ***resources and infrastructure,*** a ***pathway*** for screening, ***quality*** of screening, and ***equity*** in access to high-quality screening. The framework is used to look at how to improve each of these domains with some country examples about how this might work in practice, recognizing that some countries will move forward in a stepwise manner according to their available resources. Some brief examples of good practice from countries are also provided throughout the text.

The penultimate chapter considers important workstreams, such as governance, personnel, information systems and financing, that policy-makers may need to consider in improving or redesigning a diabetic retinopathy screening programme.

Countries in the WHO European Region face common problems in screening for diabetic retinopathy and the guide provides case studies of countries that have tackled these problems. Four important messages are delivered.

- Many low- and middle-income countries do not have enough laser capacity. The guide proposes a stepwise improvement strategy, starting with increasing laser capacity then expanding screening using available technology.
- Many countries cannot identify everyone who has a diagnosis of diabetes. Without a list of all people with a diagnosis of diabetes, some may not be invited for screening and be checked for diabetic retinopathy. Developing accurate and comprehensive lists (either nationally, regionally or locally) is another important step in improving the effectiveness of screening. For countries that do not yet have a comprehensive list(s), other steps can be taken to improve attendance, such as public awareness campaigns.
- Digital retinal photography is considered to be the most effective diabetic retinopathy screening method, but many countries cannot afford to buy cameras to screen everyone who has diabetes. This does not need to stop a screening programme developing, and while slowly increasing digital retinal camera use as resources become available, it is possible for trained and competent practitioners to screen patients using slit-lamp biomicroscopy or direct ophthalmoscopy (if slit-lamp biomicroscopy is not available).
- Many high-income countries have excellent diagnostic and treatment services, but screening pathways often are not in place for all the eligible population. Fragmented systems across family doctor, endocrinology/diabetology, ophthalmology and hospital care may mean that not everyone with diabetes regularly gets invited for screening and receives the same quality of care. A focus on pathway and quality, using integrated e-health information systems, can create a high-quality, equitable and systematic screening service for everyone with diabetes in these countries.

The guide supports policy-makers, public health leaders and senior clinicians to examine critically their current approach to diabetic retinopathy screening and challenges them, whatever their current position, to take steps to improve their approach and make diabetic retinopathy screening systematic, more effective and ultimately equitable for all people with diabetes.

References[1]

Flaxman SR, Bourne RRA, Resnikoff S, Ackland P, Braithwaite T, Cicinelli M V et al. (2017). Global causes of blindness and distance vision impairment 1990–2020: a systematic review and meta-analysis. Lancet Glob Health 5(12):e1221–34.

Lee R, Wong TY, Sabanayagam C (2015). Epidemiology of diabetic retinopathy, diabetic macular edema and related vision loss. Eye Vis. 2(1):1–25. http://dx.doi.org/10.1186/s40662-015-0026-2.

Thomas RL, Halim S, Gurudas S, Sivaprasad S, Owens DR (2019). IDF Diabetes Atlas: a review of studies utilising retinal photography on the global prevalence of diabetes related retinopathy between 2015 and 2018. Diabetes Res Clin Prac. 157:107840. https://doi.org/10.1016/j.diabres.2019.107840

WHO (2019). World report on vision. Geneva: World Health Organization (https://www.who.int/publications/i/item/world-report-on-vision).

Williams R, Airey M, Baxter H, Forrester J, Kennedy-Martin T, Girach A (2004). Epidemiology of diabetic retinopathy and macular oedema: a systematic review. Eye 18(10):963–83.

Wilson JMG, Jungner G (1968). Principles and practice of screening for disease. Geneva: World Health Organization:34 (Public Health Papers 34; https://apps.who.int/iris/handle/10665/37650).

[1] All weblinks accessed 19 October 2020.

1 Introduction

Diabetic retinopathy is a common complication of diabetes and is a major cause of vision impairment and blindness worldwide (WHO, 2019a) (Box 1). It is estimated that 950 000 people in the WHO European Region have vision impairment or blindness because of diabetic retinopathy (Flaxman et al., 2017).

Box 1. What is diabetic retinopathy?

It is a condition caused by diabetes that affects the retina. Blood vessels in the retina are damaged and become leaky or blocked.

Abnormal blood vessels can grow from the retina, which can bleed or cause scarring of the retina and result in permanent vision impairment or blindness.

Vision impairment most commonly occurs due to thickening in the central part of the retina (diabetic macular oedema), which can lead to irreversible vision impairment.

WHO's *Global report on diabetes* (WHO, 2016) and the *World report on vision* (WHO, 2019a) have highlighted the importance of diabetic retinopathy screening as a means of preventing blindness and vision impairment, and it is one of WHO's recommended effective interventions for noncommunicable diseases (WHO, 2017). Diabetic retinopathy screening is not carried out systematically in many countries in Europe, however, and opportunities to prevent people from developing vision impairment and blindness are being missed.

This guide is part of an initiative by the WHO Regional Office for Europe to improve the effectiveness of screening, maximize benefits and minimize harm. It is an operational guide and is not a clinical guideline. It is built on the approach to screening that has been described in the preceding documents in the series, *Screening programmes: a short guide* (WHO Regional Office for Europe, 2020a) and *Screening: when is it appropriate and how can we get it right?* (Sagan et al., 2020). Readers are encouraged to refer to these documents for further information on terminology, design, implementation and operation of screening programmes.

A note on terms used in this guide

The term ***diabetic retinopathy screening*** is used in this guide. In some countries, it is called diabetic eye screening.

Diabetic maculopathy is a particular kind of diabetic retinopathy. Screening for diabetic retinopathy always includes screening for diabetic maculopathy.

Diabetic macular oedema is a type of ***diabetic maculopathy.*** Both terms are used to indicate damage to the macula (central part of the retina).

2 Purpose of this guide

This guide is designed for policy-makers, public health leaders and senior clinicians involved in planning, designing and implementing services for people with diabetes and/or screening programmes in the WHO European Region.

Most countries of the WHO European Region have some screening or checking for diabetic retinopathy taking place. The focus of this guide therefore is on how to ***increase the effectiveness*** of a country's approach by moving from an unorganized towards a more systematic screening programme.

Each country's health-care system is different, and there is no single way to operate a diabetic retinopathy screening programme. The guide recognizes that countries work under different constraints, such as availability of cadres of clinicians and equipment, access to health facilities, finance to pay for new initiatives and competing health-care priorities. For this reason, the guide is designed to help policy-makers consider options and understand the advantages and disadvantages of different approaches to setting up and operating a programme. The options considered are evidence-based, feasible and achievable, if not for all countries, then for many.

Diabetic retinopathy screening is different to population screening programmes because it targets people who are already known to have a condition. Checking the eyes of a person with diabetes and offering appropriate treatment is an evidence-based intervention that reduces the risk of vision impairment and blindness and should be part of routine care for people with diabetes (WHO Regional Office for Europe & International Diabetes Federation, 1997).

The guide will help policy-makers review their current system of checking or screening for diabetic retinopathy and consider steps to increase its effectiveness through implementing a more systematic approach (Box 2).

Box 2. Taking an integrated approach for people with diabetes

The focus of this guide is diabetic retinopathy screening, but it does not stand alone. Rather, diabetic retinopathy screening takes place within the context of good care for people with diabetes.

Prevention and slowing the progress of diabetic retinopathy depends on good diabetes management. Providing patient education, supporting self-care, and facilitating the control of blood sugar, blood pressure and blood lipids through healthy lifestyles and appropriate treatment can help achieve good health outcomes and quality of life, as outlined in WHO guidance.

Health-care workers and care systems should not operate in silos. Relevant information about diabetes and eye status should be shared with the person with diabetes and across the system to facilitate integrated care. Results of eye screening should be shared with those responsible for diabetes care, and any incidental findings during eye screening, such as cataract or glaucoma, should be referred appropriately to eye-care services (WHO, 2020).

An explanation of technical terms used in the guide is provided in Annex 1.

4

Background information: diabetic retinopathy screening

This chapter considers important background information about diabetic retinopathy screening, inlcuding the epidemiology of the disease, its natural history and classification, thresholds for referral and treatment, and prevention and treatment of retinopathy.

4.1. Epidemiology

About 64 million people in the European Region have diabetes (NCD Risk Factor Collaboration, 2016), or about 7% of the population of the Region. It is estimated that 950 000 people in the WHO European Region have vision impairment or blindness because of diabetic retinopathy (Flaxman et al., 2017).

Diabetic retinopathy is a leading cause of preventable vision impairment and blindness in the working-age population (Cheung et al., 2010; Ding et al., 2012; Leasher et al., 2016). The economic burden of vision impairment and blindness due to diabetic retinopathy in Europe is considerable (Happich et al., 2008; Heintz et al., 2010).

A global study in 2017 found that of the leading causes of vision impairment and blindness, the crude global prevalence (all ages) of diabetic retinopathy as a cause increased between 1990 and 2015, while all other causes of vision impairment and blindness decreased markedly (Flaxman et al., 2017).

The prevalence of diabetic retinopathy in people with diabetes varies according to the type of diabetes, how long they have had the condition, and by region. Which test is chosen to measure prevalence and what is measured can also affect the amount of disease reported. This means that ranges of values for prevalence of diabetic retinopathy reported can differ significantly between studies. In Europe, it is estimated that between 20% and 35% of people with diabetes will have any form of diabetic retinopathy and approximately 2% will have proliferative diabetic retinopathy; for macular oedema among people with type 2 diabetes, the estimates vary widely between 1% and 13%, depending on how it is measured (Williams et al., 2004; Lee et al., 2015; Thomas et al., 2019).

Diabetic retinopathy is an important health problem

Wilson & Jungner's 1st principle

4.2. How diabetes causes diabetic retinopathy

Fig. 1 shows the structure of the eye. The retina is the area at the back of the eye that receives light, transforming it to nervous impulses. The macula is the central part of the retina that allows us to see fine detail and colours.

Diabetic retinopathy is a direct consequence of raised glucose levels on the small blood vessels of the retina. Other important risk factors for diabetic retinopathy are raised blood pressure and elevated serum lipids, both of which are common in people with diabetes.

People with diabetic retinopathy may not have any symptoms of vision impairment (asymptomatic).

When a person has the most advanced form of diabetic retinopathy, they can ***suddenly*** develop severe vision impairment or blindness because of bleeding from abnormal retinal vessels into the eye or damage to the retina from a retinal detachment.

As diabetic macular oedema increases in severity, the thickening of the retina affects the central part of the macula. This damage can occur more slowly than in proliferative diabetic retinopathy, leading to ***progressive*** vision impairment.

Fig. 1. The eye

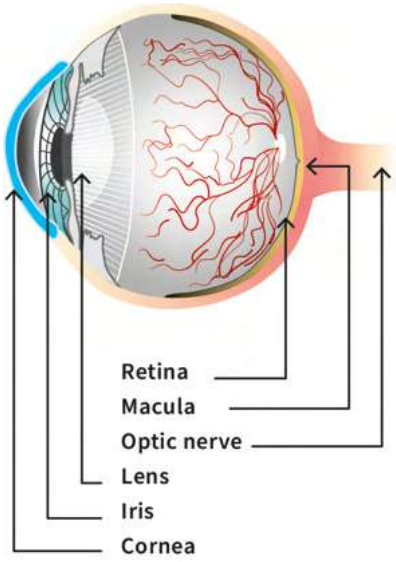

Source: adapted from WHO (2019a).

4.3. Natural history and classification of diabetic retinopathy

The natural history of diabetic retinopathy was described in a pivotal study called the Early Treatment Diabetic Retinopathy Study (ETDRS) carried out in the 1980s (Early Treatment Diabetic Retinopathy Study Research Group, 1991). The description of disease progression in the ETDRS is still used today as the basis for classification systems for diabetic retinopathy.

Classification and grading systems ***classify*** findings on examination using agreed nomenclature and then ***grade*** them according to severity.

One example of a classification system based on the ETDRS can be found in the International Council of Ophthalmology (ICO) guidelines for diabetes eye care (International Council of Ophthalmology, 2017; Wong et al., 2018).

The classification distinguishes between retinopathy and maculopathy because they can progress at different rates and changes in the macula can occur at all grades of severity of diabetic retinopathy.

A simplified version of this classification system is given in Fig. 2a and 2b. The full version of the ICO classification can be found in Annex 2.

The natural history of diabetic retinopathy is adequately understood and there is a recognizable latent or early symptomatic phase

Wilson & Jungner's 4th and 7th principles

Fig. 2a. Diabetic retinopathy classification

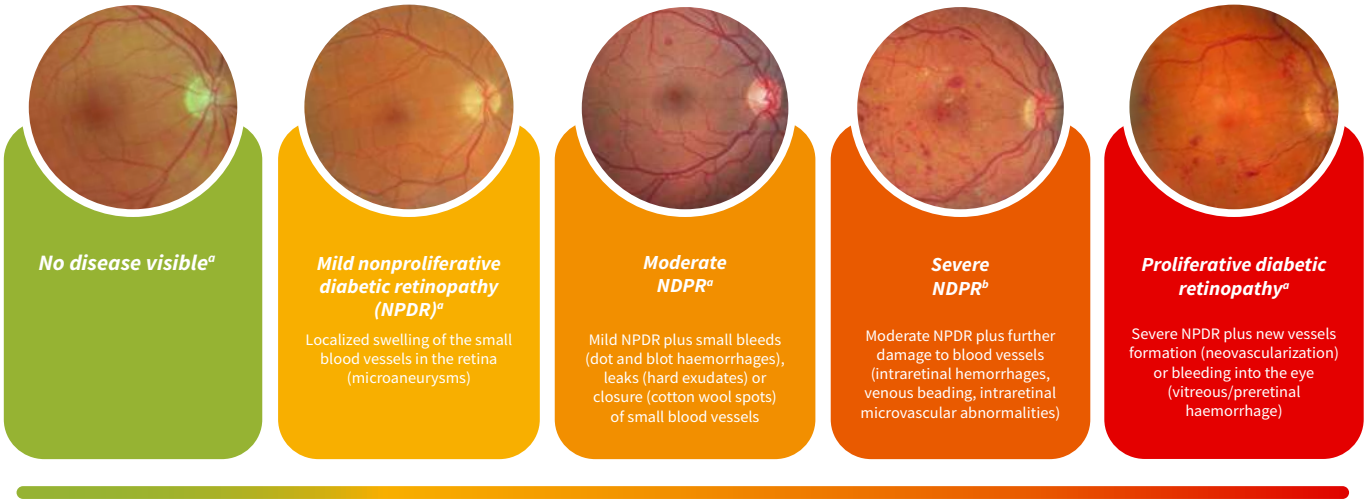

Note: the description of each grade is simplified. For full descriptions, see Annex 2.

[a] Photograph © Simon Harding.
[b] Photograph © Vittorio Silvestre.

Source: International Council of Ophthalmology (2017).

Fig. 2b. Diabetic macular oedema classification

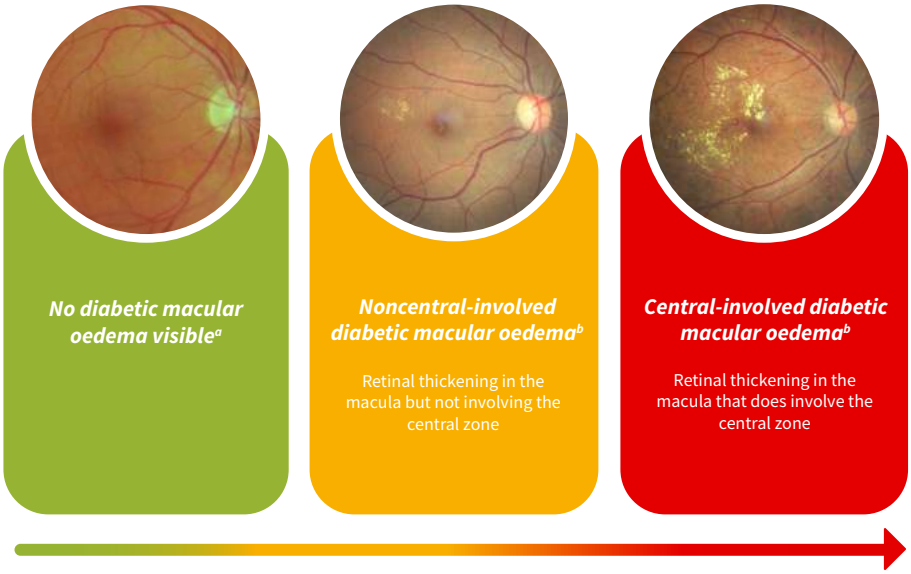

Note: the description of each grade is simplified. For full descriptions, see Annex 2.

[a] Photograph © Simon Harding.
[b] Photograph © Vittorio Silvestre.

Source: International Council of Ophthalmology (2017).

The diabetic retinopathy severity classification (grade) indicates the risk of a person developing the most advanced form of sight-threatening diabetic retinopathy.

Policy-makers should work with clinicians to discuss which detailed classification and grading system is in use in their country and if any amendment or change is required.

4.4. Prevention and treatment of diabetic retinopathy

Good blood glucose control and control of blood pressure and elevated lipids reduces the risk of new-onset diabetic retinopathy and slows progression of existing diabetic retinopathy (Diabetes Control and Complications Trial Research Group, 1993; Turner et al., 1998; Yau et al., 2012). This approach should underpin the prevention and treatment of diabetic retinopathy in all people with diabetes.

Laser treatment is the mainstay of treatment for proliferative diabetic retinopathy and can also be used for the treatment of diabetic macular oedema (Wong et al., 2018).

Anti-VEGF (vascular endothelial growth factor) agents and steroids injected into the eye can reduce the progression of the disease and preserve visual function in diabetic macular oedema (Wong et al., 2018). There are several anti-VEGF agents, and bevacizumab is included in the WHO Model List of Essential Medicines (WHO, 2019b).

Vitrectomy can restore useful vision in eyes with non-resolving vitreous haemorrhage and traction retinal detachment of the macula.

There are agreed policies on whom to treat as patients and accepted evidence-based treatments for patients with diabetic retinopathy

Wilson & Jungner's 2nd and 8th principles

Policy-makers are referred to the ICO guidelines on diabetic eye care (International Council of Ophthalmology, 2017) for further evidence-based recommendations on the treatment of diabetic retinopathy and maculopathy based on resource settings (Wong et al., 2018).